Loss of cardiomyocyte eukaryotic elongation factor 1 A2 in adult mice triggers cardiomyopathy due to defective proteostasis

Abel Martin-Garrido[1], Nadine Weyrauch[1], Jorge Ruiz-Orera[2], Jeanette Eresch[1], Sonja Reitter[3], Julio Cordero[4], Viktoria Scheich[1], Andrea Grund[1], Merve Keles[1], Nina Weinzierl[1], Ellen Hofmann[1], Felix A. Trogisch[1], Shruthi Hemanna[1], Georg Stoecklin[3], Mirko Völkers[5], Norbert Hübner[2,6,7,8], Gergana Dobreva[4,8,9] and Joerg Heineke[1,8,9,§]

[1]Department of Cardiovascular Physiology, European Center for Angioscience (ECAS), Medical Faculty Mannheim, Heidelberg University, Mannheim, Germany

[2]Cardiovascular and Metabolic Sciences, Max Delbrück Center for Molecular Medicine in the Helmholtz Association (MDC), Berlin, Germany.

[3]Department of Biochemistry, Mannheim Institute for Innate Immunoscience (MI3), Medical Faculty Mannheim, Heidelberg University, Mannheim, Germany

[4]Department of Cardiovascular Genomics and Epigenomics, European Center for Angioscience (ECAS), Medical Faculty Mannheim, Heidelberg University, Mannheim, Germany

[5]Department of Internal Medicine III, Heidelberg University, Heidelberg, Germany;

[6]DZHK (German Center for Cardiovascular Research), Partner Site Berlin, Berlin, Germany.

[7]Charité-Universitätsmedizin, Berlin, Germany.

[8]Helmholtz Institute for Translational AngioCardioScience (HI-TAC) of the Max Delbrück Center for Molecular Medicine in the Helmholtz Association (MDC) at Heidelberg University, Heidelberg, Germany.

[9]DZHK (German Center for Cardiovascular Research), partner site Heidelberg/Mannheim

[§]**Corresponding Author:** Joerg Heineke, Professor of Cardiovascular Physiology at Heidelberg University, Director, Department of Cardiovascular Physiology, Co-director, European Center for Angioscience, Medical Faculty of Mannheim, Heidelberg University, Email: Joerg.Heineke@medma.uni-heidelberg.de, Phone: +49 (0)621 383 71855

Abstract

The eukaryotic elongation factor 1A (eEF1A) is known for its canonical role to promote the translocation of aminoacyl-tRNAs to ribosomes during translational elongation, but also has non-canonical functions. In mammals, two paralogs of eEF1A exist: Whereas eEF1A1 is ubiquitously expressed, eEF1A2 expression is restricted to adult cardiomyocytes, skeletal myocytes and neurons. Although patients with mutations in *EEF1A2* develop cardiomyopathies, the mechanism involved is unknown. To study the role of cardiac eEF1A2 in adult mice, we generated adult induced, cardiomyocyte specific *Eef1a2* knock-out (eEF1A2-cKO), and *Eef1a1/Eef1a2* double knock-out (eEF1A1/eEF1A2-cKO) mice. eEF1A2-cKO mice developed cardiomyopathy associated with increased mouse mortality, cardiac dysfunction and fibrosis, but unchanged global protein synthesis rates, while eEF1A1/eEF1A2-cKO mice exhibited early sudden death. Combined RNA sequencing, proteomics and ribosomal sequencing analyses from hearts of eEF1A2-cKO and eEF1A1/eEF1A2-cKO mice revealed a post-transcriptional upregulation of ribosomal proteins and translational regulators. On the other hand, we observed an increase of autophagosomes and protein aggregates in heart tissue of eEF1A2-cKO mice as sign of defective autophagy. Mechanistically, we demonstrate that eEF1A2 acts as a chaperone in cardiomyocytes. Finally, administration of rapamycin (mTORC1 inhibitor) at an early disease stage in eEF1A2-cKO mice normalized systolic cardiac dysfunction and mortality and eliminated the accumulation of autophagosomes and protein aggregates. Together, we found that eEF1A2 promotes proteostasis in cardiomyocytes, at least in part by supporting protein folding. More importantly, increased mortality, cardiomyopathy and proteostasis defects due to the lack of eEF1A2 could be rescued by administration of rapamycin, which might therefore constitute a treatment strategy for patients with EEF1A2 mutations.

Introduction

The eukaryotic elongation factor 1A (eEF1A) is present as two paralogous isoforms, eEF1A1 and eEF1A2, which share a high degree of sequence homology (92% at the mRNA level and 98% at the protein level)[1]. Its canonical role is to facilitate the GTP-dependent delivery of aminoacyl–transfer RNAs to the ribosome, a process that is essential for the fidelity and efficiency of polypeptide synthesis during the elongation phase of translation [2, 3].

During postnatal development, a well-characterized isoform switch occurs in skeletal muscle cells, neurons, and cardiomyocytes, where the fetal eEF1A1 is replaced by the adult paralog eEF1A2 [4-6]. In contrast, most other cell types continue to express eEF1A1 throughout adulthood. The functional importance of this developmental switch was first elegantly demonstrated by Cathy Abbott's lab, which showed that the "wasted" mutation—an autosomal recessive deletion of the *Eef1a2* gene—results in weight loss, progressive paralysis, and premature death around 28 days after birth [5]. More recently, Feng et al. provided further evidence of eEF1A2's essential role by demonstrating that cardiomyocyte-specific neonatal deletion of *Eef1a2* leads to cardiomyopathy and premature death between 7 and 22 weeks after birth [7].

eEF1A is one of the most abundant intracellular proteins, accounting for approximately 1% to 11% of the total cellular proteome [3]. A previous study in rabbit reticulocytes has estimated an eEF1A-to-ribosome ratio of 17–35:1 and an eEF1A-to-tRNA ratio of 13:1, indicating that free eEF1A is the most prevalent form [3]. Given this abundance, it is not surprising that eEF1A is also involved in different non-canonical cellular processes. These include actin polymerization, proteasome activity, viral replication, protein folding, and cell proliferation [8]. Notably, eEF1A2 exhibits patterns of translation buffering in human hearts and non-human primates, highlighting the importance of maintaining protein expression [9].

Recently, Cao et al. reported the first known case of a homozygous *EEF1A2* missense mutation (P333L) in humans, associated with cardiomyopathy, epilepsy, global developmental delay, and early mortality [10]. Furthermore, Feng et al. generated a knock-in mouse model, in which the endogenous cardiac *Eef1a2* gene was replaced with the P333L variant [7]. Despite exhibiting *Eef1a2* mRNA levels comparable to wild-type controls, mutant mice showed a marked reduction in eEF1A2 protein levels in cardiac tissue, suggesting that the P333L substitution compromises protein stability and functions as loss-of-function mutation. Indeed, cardiac-specific P333L-*Eef1a2* mice and neonatal onset *Eef1a2* knockout (KO) mice were phenotypically indistinguishable. Both lines began to exhibit mortality from 8 weeks of age, with complete lethality by 17 weeks. Interestingly, global cardiac protein synthesis was unaffected in P333L-*Eef1a2* and *Eef1a2* KO hearts, suggesting that the cardiomyopathy observed in both models might be independent of the canonical function of eEF1A2, but the molecular mechanisms of how the loss of eEF1A2 leads to heart disease remained largely unknown.

In this study, we investigate the role of eEF1A in adult cardiomyocytes. Our results show that deletion of *Eef1a2* in adult cardiomyocytes in mice leads to cardiomyopathy, with a lethality rate of 45% observed two months post gene-deletion. Furthermore, we demonstrate that eEF1A1 plays a protective role in the absence of eEF1A2, as mice with cardiomyocyte-specific deletion of both *Eef1a1* and *Eef1a2* exhibit complete lethality within six weeks after gene-deletion. Mechanistically, by combining mRNA sequencing, proteomics, and ribosomal sequencing analyses, we demonstrate an upregulation in the protein expression of 5'-TOP mRNA genes in eEF1A2-deficient hearts. In addition, we identify eEF1A2 as a critical chaperone involved in cardiac protein folding. Interestingly, treatment with rapamycin almost completely rescued cardiac dysfunction and reduced the accumulation of misfolded proteins caused by *Eef1a2* deletion, offering a potential tailored therapeutic approach for patients with inherited *EEF1A2* mutations. In summary, our findings identify eEF1A2 as a crucial

regulator of cardiac proteostasis, essential for maintaining protein homeostasis in adult cardiomyocytes independent of its canonical role in the protein synthesis.

Results

Adult induced deletion of *Eef1a2* in cardiomyocytes leads to cardiomyopathy

Previous findings indicate that *Eef1a2* expression is essential for maintaining cardiac function during postnatal heart development. However, the role of eEF1A2 in adult cardiomyocytes remains unknown [7]. To investigate the function of eEF1A2 in the adult heart, we generated a cardiomyocyte-specific, tamoxifen-inducible conditional knockout mouse model (eEF1A2-cKO) by interbreeding αMHC-MerCreMer with newly generated Eef1a2 flox/flox mice. Tamoxifen was administered to mice aged 6–7 weeks to induce Cre recombinase activity and specifically delete *Eef1a2* in cardiomyocytes. Eef1a2 flox/flox mice (littermates) were used as control (Eef1a2-WT). Our results show that eEF1A2-cKO mice began to exhibit mortality at 6 weeks after tamoxifen injection, with a 50% survival rate observed at two months (Figure 1A). Cardiac systolic function, assessed as ejection fraction in echocardiography, showed no significant differences between control and eEF1A2-cKO mice at one month post-deletion (Figure S1A). However, by two months, eEF1A2-cKO hearts displayed marked cardiac dysfunction, with an approximately 60% reduction in left ventricular ejection fraction compared to control mice (Figure 1B). Gravimetric analysis at two months after Tamoxifen injection revealed significant enlargement of both ventricles and atria in eEF1A2-cKO mice (Figure 1C), which were not detectable one month earlier (Figure S1B). Cardiac hypertrophy in eEF1A2-cKO mice was accompanied by an increase in cardiomyocyte cross-sectional area, indicative of cellular hypertrophy (Figure 1D). Furthermore, Sirius red staining indicated advanced myocardial fibrosis two months after tamoxifen injection in eEF1A2-cKO mice, which started to emerge already at the one month time point (Figure 1E, S1D). Analysis of hypertrophic gene expression revealed a significant upregulation as early as one month post-tamoxifen administration (Figure S1E), which was further enhanced at two months (Figure 1F). Finally, given that eEF1A2 is canonically involved in the elongation phase of protein synthesis, we investigated whether its deletion affects global protein synthesis. Using a puromycin incorporation assay, we found no significant differences in global protein synthesis between eEF1A2-cKO and control isolated cardiomyocytes at one or two months post gene-deletion (Figure 1G-H and S1F). Viability, cardiac function, and morphology were similar at one, two, and 4 months after tamoxifen administration in αMHC-MerCreMer mice on a wild-type background, demonstrating that the effects observed in Eef1a2-cKO mice were due to the deletion of *Eef1a2*, and not to tamoxifen-induced Cre activation (data not shown). Collectively, our results demonstrate that deletion of eEF1A2 in adult cardiomyocytes induces progressive cardiac dysfunction and mouse mortality between one and two months after initiating deletion of the gene, while general protein synthesis activity was not affected.

Combined adult onset ablation of *Eef1a1* and *Eef1a2* leads to early sudden death

Western blot analysis of the different eEF1A paralogs in the heart revealed that a compensatory upregulation of *Eef1a1* occurred in isolated cardiomyocytes upon *Eef1a2* deletion as early as one month after tamoxifen administration (Figure 1G and S1F). To assess the functional significance of this upregulation, we generated cardiomyocyte-specific, tamoxifen-inducible conditional double knockout mice lacking both *Eef1a1* and *Eef1a2* (eEF1A1/eEF1A2-cKO). Our results show 100% mortality between 40 and 45 days post-tamoxifen in eEF1A1/eEF1A2-cKO mice (Figure 2A). Interestingly, echocardiographic assessment at one month post-tamoxifen, showed no signs of cardiac dysfunction, but a small reduction in diastolic and systolic left ventricular dimensions in double knockout mice (Figure 2B and data not shown). In line with this observation, gravimetric analysis (Figure 2C) and

morphological assessment cardiomyocyte cross-sectional area (Figure 2D) revealed no significant differences between eEF1A1/eEF1A2-cKO and control mice (littermate Eef1a1flox/flox; Eef1a2flox/flox mice). Furthermore, no cardiac fibrosis was observed in the double knock-out hearts at that time point around 10 days before mortality started (Figure 2E). However, analysis of hypertrophic gene expression revealed a significant dysregulation of all analyzed genes (except for Actc1) (Figure 2F), which appeared to be more pronounced than that observed in eEF1A2-cKO mice at the one month time point (Figure S1E). Notably, in contrast to the single eEEF1A2 knockout, puromycin incorporation was significantly reduced by about 30% in cardiomyocytes and cardiac tissue (not shown) from eEF1A1/eEF1A2-cKO mice, indicating mildly impaired global protein synthesis (Figure 2G). We next analyzed mice with adult induced cardiomyocyte specific *Eef1a1* knock-out (eEF1A1-cKO). As shown in Figure S2, viability, cardiac function, and morphology remained unchanged at one, two, and four months after Tamoxifen application, demonstrating that cardiac eEF1A1 expression is dispensable under physiological conditions in adulthood, when eEF1A2 is the predominant paralog. Altogether, these results demonstrate on one hand that the upregulation of eEF1A1 observed in eEF1A2-cKO mice is compensatory and on the other hand that eEF1A1 and eEF1A2 are at least partially functionally interchangeable in cardiomyocytes, particularly in maintaining protein synthesis.

Increased translation of ribosomal proteins upon *Eef1a2* gene deletion

Next, we investigated the potential mechanisms underlying cardiac dysfunction induced by *Eef1a2* knock-out. We performed both proteomic and RNA-seq analyses on whole heart tissue one month after tamoxifen mediated gene deletion, in order to capture initial molecular changes that occur prior to the onset of cardiac dysfunction. RNA-seq analysis revealed upregulation of muscle, sarcomeric, hypertrophic and unfolded protein response genes as well as downregulation of genes involved in action potential generation, endothelial proliferation, muscle contraction and potassium transport (Figure S3A-B). Interestingly, proteomic analysis uncovered a marked upregulation of ribosomal subunit proteins and translation regulatory factors, as well as a downregulation of lipid oxidation, fatty acid and carboxylic acid metabolic process related proteins (Figure S3C-D).

Given the heterogeneous cell composition of the heart, we next sought to validate these proteomic findings in isolated cardiomyocytes. For this purpose, we isolated adult cardiomyocytes from eEF1A2-cKO, eEF1A1/A2-cKO and the respective control mice one month after tamoxifen injections and subjected them to proteomic analyses (Figure 3A). Proteins identified in cardiomyocytes of both knock-out mouse lines were also compared with the results from cardiomyocytes isolated from αMHC-MerCreMer transgenic mice (Figure S4A). Proteins that exerted similar levels in all groups were removed from the list. As shown in Figure 3B, we identified 40 differentially expressed proteins in eEF1A2-cKO, and 301 in eEF1A1/eEF1A2 double-cKO cardiomyocytes (Figure 3D). Gene Ontology (GO) analysis confirmed an upregulation of ribosomal subunits and translation regulatory factors in eEF1A2-cKO, which was even more pronounced in the double-cKO cardiomyocytes (Figure 3C and E and Figure S4B-C). Notably, 95% of the differentially expressed proteins in the EEF1A2-cKO group were also observed in the double-cKO, but they represented only 20% of the total changes seen in the double knockout (Figure 3F). To validate these findings, we performed Western blotting for Eef2 and RpS6, as examples for translation regulatory factors and ribosomal subunits, respectively. As shown in Figure 3G and H, we observed an upregulation of Eef2 and RpS6 protein in isolated cardiomyocytes from eEF1A2-cKO and eEF1A1/A2-cKO mice within one month after tamoxifen administration. mRNA levels of Rps6 and Eef2, in contrast were not significantly changed. In addition, Eef1a1 mRNA was not altered in eEF1A2-cKO cardiomyocytes (Figure S4D).

The observation that the total protein of ribosomal subunits and translation regulatory factors (including Eef2 and eEF1A1) are upregulated without an increase in mRNA, suggested that this effect

might be mediated post-transcriptionally. To verify this, we performed ribosomal sequencing (Ribo-Seq) to measure ribosome-protected mRNA fragments from actively translating ribosomes in isolated hearts one month after tamoxifen injections (Figure 3I). Ribo-Seq showed that ribosomal subunits and translation factors RNAs exerted the highest increase in ribosomal reads in eEF1A2- and eEF1A1/eEF1A2-cKO hearts compared with controls (Figure S5A-B). More importantly, when translational efficiency (TE) was calculated by normalizing ribosomal reads of a gene to its mRNA expression in the same sample, ribosomal subunits and translation factors were again among the most upregulated gene groups in both knock-out mouse lines (Figure 3J-K). Of note, a principal component analysis of TE values clearly distinguished each experimental group (Figure S6A). Consistent with our proteomics findings, we observed a synergistic increase in TE for ribosomal subunits and translation factors in the eEF1A1/eEF1A2-cKO hearts compared with the eEF1A2-cKO hearts (Figure S5C). We also performed an analysis of mRNA codon usage. No major differences were observed in eEF1A2-cKO hearts. In contrast, Asparagine (N), Glycine (G) and Leucine (L) codon usage levels were slightly reduced in eEF1A1/eEF1A2-cKO, while Lysine (K), Proline (P) and Arginine (R) codon usage levels were increased. This result suggested that N, G and L codons are more efficiently decoded, whereas K, P and R codons are decoded more slowly in eEF1A1/eEF1A2-cKO hearts (Figure S6B). Collectively, we found that eEF1A regulates protein expression of ribosome subunits and translation factors in cardiomyocytes at the post-transcriptional level.

Next, we investigated whether the upregulation of ribosomal subunits and elongation factors altered the monosome and polysome ratio and the spatial regulation of protein synthesis, as this had been previously shown to be critical for proper cardiac function [11-13]. We therefore isolated and quantified monosome and polysome fractions using sucrose gradient centrifugation, but no differences were observed in the monosome-to-polysome ratios between control, eEF1A2-cKO and eEF1A1/eEF1A2-cKO hearts (Figure S7A-B). Similarly, the distribution of RpS6 (a representative ribosomal subunit), Eef2 (a representative elongation factor), Eif2α (a representative initiation factor) and EDF1 (a marker of ribosome collisions [14, 15]) across monosome and polysome fractions was similar (Figure S7C-D). The Z-disc has been reported to serve as an anchor for protein synthesis in adult cardiomyocytes. Accordingly, staining for eEF1A2 revealed a sarcomeric staining pattern, which was lost in eEF1A2-cKO cardiomyocytes (Figure S8). Immunofluorescence analysis of the ribosomal protein RpS6 together with the Z-disc protein α-actinin in isolated cardiomyocytes from EEF1A1/a2-cKO mice revealed no differences in RpS6 localization compared with WT controls (Figure S8 and S9). In summary, our results indicate that the protein synthesis machinery and its subcellular localization remain unaltered after deletion of EEF1A2, suggesting that the deleterious cardiac effects observed are not due to mis localization of protein synthesis.

mRNAs encoding ribosomal subunits, as well as translation initiation and elongation factors, contain a 5' terminal oligopyrimidine tract (5'TOP) motif at their 5' end, hereafter termed 5'TOP mRNAs [16]. Multiple studies have shown that the translation of 5'TOP mRNAs is regulated by mTORC1 activity [17-20]. We next investigated whether mTORC1 activity is affected by the deletion of eEF1A2, using phosphorylation of RpS6 at Ser240/244 as a commonly used surrogate marker for mTORC1 activity, given that this phosphorylation is largely dependent on the mTORC1–S6K1 signaling pathway. To explore the potential involvement of mTORC1 in the cardiac dysfunction observed in eEF1A2-cKO mice, we analyzed heart samples collected two months after eEF1A2 deletion, a time point at which reduced cardiac function was evident (Figure 1B). We found that total RpS6 as well as relative phosphorylation of RpS6 were upregulated at this time point (Figure 4A-B). Moreover, immunofluorescence staining confirmed that phosphorylation of RpS6 occurred mainly in cardiomyocytes by co-staining phospho-RpS6 with α-actinin, a cardiomyocyte specific marker (Figure 4C). Notably, Eef2 was similarly

upregulated in eEF1A2-cKO cardiac tissue (Figure S10A-B). However, the ratio of phospho-Eef2 versus total Eef2 remained unaltered.

Accumulation of autophagosomes and misfolded proteins in the myocardium of eEF1A2-cKO mice

Autophagy is an essential process responsible for the removal of misfolded or aggregated proteins and the clearance of damaged organelles. Previous studies have shown that mTORC1 activity negatively regulates autophagy [21]. p62 is an adaptor protein involved in selective autophagy playing a key role in the clearance of protein aggregates and organelles via macroautophagy [22]. As shown in Figure 4A, we observed an increase in p62 protein levels in EEF1A2-cKO, suggesting impaired macroautophagic activity. Macroautophagy is a multistep and complex process, and one crucial regulatory step is the conversion of cytosolic LC3B (LC3-I) to its lipidated, autophagosome-associated form (LC3-II). To further investigate this, we analyzed the levels of LC3-I and LC3-II. Interestingly, we observed an increase in LC3-I and LC3-II levels (Figure 4D-E). In addition, we observed an increase in Beclin1 and Atg7 (Figure 4D-E), critical components of the multiprotein complex that participates in vesicle nucleation and the processing of LC3-I to LC3-II.

Given that our results suggest a deficit in macroautophagic activity in eEF1A2-cKO hearts, we next investigated whether protein aggregates accumulate in these hearts. Using a specific probe (Proteostat) to detect aggregated proteins, we observed that between 20% and 30% of cardiomyocytes in eEF1A2-cKO hearts contained protein aggregates, whereas none were detected in control (WT) hearts (Figure 4F-G). Moreover, co-staining with p62 in cardiac tissue revealed that approximately 50–60% of Proteostat-positive cardiomyocytes were also positive for p62. Conversely, among the p62-positive cardiomyocytes (between 10 to 20% of the total CM), around 70% were also Proteostat-positive (Figure S10D). Moreover, the p62 bodies were ubiquitin positive, indicating that ubiquitination preceded inclusion of degradation prone protein into autophagic vacuoles (Figure 4H). In contrast, although within the same cell, p62 and Proteostat staining as well as ubiquitin and Proteostat appeared spatially separated, suggesting the labelling of mutually exclusive processes, whereby proteins that cannot enter autophagosomes end up in Proteostat positive protein aggregates (Figure 4F, Inset, Figure S11). Electron microscopy revealed largely unaltered sarcomere and mitochondrial morphology, an accumulation of autophagosomes, but not autolysosomes in cardiomyocytes of eEF1A2-cKO versus control mice, again pointing towards a defect in autophagic flux due to eEF1A2 deletion (Figure 4I).

eEF1A2 acts as chaperone in cardiomyocytes

Several studies have demonstrated a chaperone-like activity of eEF1A in vitro [23-25]. To investigate whether the increased levels of misfolded proteins that we observed in our model could be due to a loss of this activity, we performed a luciferase-based protein folding assay. For this, we isolated CM from WT, eEF1A2-cKO, and eEF1A1/eEF1A2-cKO mouse hearts one month after tamoxifen administration (Figure 5A). These CMs were transduced with adenoviruses expressing firefly luciferase (under the SV40 promoter) and Renilla luciferase (under the thymidine kinase promoter) [26]. Our results showed a significant reduction in luciferase activity in CMs from eEF1A2-cKO and double cKO mice. More specifically, firefly luciferase activity decreased by ~80% and Renilla luciferase activity by ~40% compared to WT CMs (Figure 5B, D). This reduction in luciferase activity was not due to differences in transcriptional activity, as luciferase mRNA levels were similar across all groups (Figure 5C, E). Additionally, protein synthesis appeared largely unaffected in eEF1A2-cKO CMs (Figure 1G-H) and was only slightly decreased in the double cKO (Figure 2G, I), suggesting that reduced translation alone does not account for the observed effects and implying either reduced protein synthesis fidelity or defective protein folding as potential mechanisms. Since eEF1A has been implicated in maintaining protein fidelity [27, 28], we tested whether the decrease in luciferase activity might be due to increased

amino acid misincorporation or stop codon read-through. To assess this, we transduced CMs with adenoviruses encoding mutant firefly luciferase constructs carrying either the R216S substitution or a premature stop codon at position 210, along with WT Renilla luciferase as an internal control. As shown in Figure S12A-D, the activity of mutant firefly luciferase (R218S or STOP) was undetectable after normalization to Renilla, in knock-out similar to wild-type CMs, indicating that misincorporation or read-through is unlikely to explain the reduction in luciferase activity. Accumulation of misfolded proteins has been shown to trigger the Unfolded Protein Response (UPR). We therefore analyzed phosphorylation of the eukaryotic initiation factor 2 α (Eif2α) in cardiac tissue, which is a common feature of the UPR. As shown in Figure 5F-H, we observed an increase in phospho-Eif2α as well as total Eif2α 2 months after eEF1A2 deletion. To investigate whether eEF1A2 can function as a molecular chaperone promoting protein folding, we generated a HEK293 cell line constitutively expressing eEF1A2 under the control of the CMV promoter using CRISPR/Cas9 technology. As shown in Figure S12E, we successfully isolated two independent clones that overexpress eEF1A2. Importantly, overexpression of eEF1A2 did not affect the expression levels of eEF1A1, which is the predominant paralog in HEK293 cells. We transfected the cells with a plasmid encoding both Firefly and Renilla luciferase and performed a luciferase unfolding/refolding assay (Figure 5I). Cells were subjected to a heat shock (43°C for one hour), and luciferase activities were measured immediately afterwards (unfolding assay), as well as after 1 and 3 hours of recovery (refolding assay). Our results showed that eEF1A2 overexpression partially protected both luciferases from heat-induced unfolding compared to wild-type or non-targeted control cells. Furthermore, the refolding of luciferase enzymes was accelerated in eEF1A2-overexpressing cells, with significant increased activity at 1 hour for both luciferases and at 3 hours for Renilla luciferase (Figure 5J-K).

Altogether, we demonstrate for the first time that eEF1A2 acts as a chaperone in vivo, and its loss leads to reduced folding efficiency of client proteins such as luciferase as well as activates the UPR in cardiomyocytes.

Rapamycin treatment partially rescues cardiomyopathy in eEF1A2-cKO mice

We hypothesized that defective autophagy with accumulation of autophagosomes and misfolded proteins in around 20% of cardiomyocytes might play a causative role in the development of cardiomyopathy in eEF1A2-cKO mice. Because increased mTOR activation as indicated by increased Rps6 phosphorylation was a potential reason for defective autophagic flux in these mice, we investigated whether pharmacological inhibition of mTOR might have beneficial effects. Treatment with the mTOR inhibitor Rapamycin was therefore initiated one month after tamoxifen administration—a time point at which cardiac function was still comparable between eEF1A2-cKO and wild-type (WT) mice, although eEF1A2 protein was already completely lost in the hearts of the knock-out animals (Figure 6A). As shown in Figure 6B, daily administration of Rapamycin for one month completely reversed the increased mortality in eEF1A2-cKO mice. Rapamycin fully restored systolic cardiac function and reversed cardiac hypertrophy (Figure 6C-F). Interestingly, despite these improvements, cardiac fibrosis remained unaffected (Figure 6G). To better understand how Rapamycin affected cardiac function in eEF1A2-cKO mice, we analyzed global protein synthesis, phosphorylated Rps6 abundance, autophagosome, protein aggregates and fibrosis in the heart. As shown in Figure 6H-I, protein synthesis remains similar between the control and Rapamycin-treated groups. The abundance of representative 5'TOP mRNA encoded proteins (including RpS6, Eef2, and RpS15) as well as of Atg7 and Beclin1 were not significantly different between vehicle- and Rapamycin-treated eEF1A2-cKO hearts, despite a complete ablation of RpS6 phosphorylation following Rapamycin treatment (Figure 7A-C, S13A-D). In contrast, Rapamycin led to a significant reduction in p62 and LC3-I proteins in the heart. This effect was accompanied by a decrease in Proteostat and p62 positive cardiomyocytes compared to the vehicle-treated group (Figure 7D-E). Notably, we also observed a

reduction in the expression of phospho-EIf2α and total EIf2α in response to Rapamycin, demonstrating that it relieves the UPR response in eEF1A2-cKO cardiomyocytes (Figure 7A-B).

In summary, our results indicate that the loss of eEF1A2 impairs cardiac proteostasis, contributing to cardiac dysfunction. Moreover, restoration of the cardiac proteostasis by Rapamycin largely reversed the associated cardiac pathology in eEF1A2-cKO hearts.

Discussion

One key observation from our study was the completely unaltered global protein synthesis activity in eEF1A2-cKO mice, despite the complete absence of eEF1A2 in cardiomyocytes. A previous report noted increased eEF1A1 protein expression in eEF1A2-knockout hearts; however, the underlying mechanisms and physiological significance were unknown. Here, we demonstrate for the first time that EEF1A2 regulates EEF1A1 at the post-transcriptional level, and that the upregulation of eEF1A1 serves as a compensatory mechanism. This is supported by our finding that double conditional knockout (cKO) of both eEF1A1 and eEF1A2 led to mildly reduced global protein synthesis and 100% mortality approximately 6–7 weeks after gene deletion. Our results support the current paradigm that eEF1A1 and eEF1A2 expression is mutually exclusive, but also reveal a previously unrecognized layer of regulatory interaction between these two paralogs in the heart.

Protein synthesis varies significantly across organs and developmental stages. During postnatal cardiac development, it is markedly reduced, making adult cardiac tissue one of the organs with the lowest protein synthesis rates [29]. Moreover, this downregulation coincides with the upregulation of eEF1A2 expression in the heart. This inverse correlation suggests that eEF1A2 may serve non-canonical functions in the cardiac context. Previous studies have shown that during translation, eEF1A remains associated with nascent polypeptides and that it interacts with damaged proteins and facilitate their degradation via the proteasome [24, 30, 31]. This suggested that eEF1A2 might play a role in protein quality surveillance by assisting in protein folding and clearance of misfolded proteins. We observed protein aggregate formation and an mRNA-independent reduction in luciferase activity in cardiomyocytes lacking eEF1A2. In contrast, overexpression of eEF1A2 prevented protein unfolding and enhanced protein refolding during and after heat shock. Together, these findings demonstrate that eEF1A2 functions as a physiologically relevant chaperone in vivo. By doing so, eEF1A2 strongly promotes cellular proteostasis.

Two important questions remain unanswered: does eEF1A2 function as an independent chaperone or as a co-chaperone, and does it exhibit specificity toward certain protein substrates? Regarding the first question, a recent study showed that eEF1A1, but not eEF1A2, transcriptionally regulates the expression of HSP70 and HSP27 after heat shock [32]. Both molecular chaperones help cells cope with stress by preventing protein misfolding and aggregation. Conversely, several studies have demonstrated a direct role for eEF1A or eEF-Tu (Thermal unstable), the bacterial homologue of eEF1A, in the in vitro folding of several proteins, supporting a direct chaperone-like function [24, 25, 33, 34]. Our results are more consistent with this latter possibility, as our Ribo-seq, RNA-seq, and proteomics analyses did not show enrichment of the heat-shock response. Nonetheless, we cannot fully exclude some contribution of HSPs in our model, especially since HSPs are playing a pivotal role in heart failure [35]. For the second question, a previous work has shown that eEF1A associates with nascent polypeptides independently of the Nascent Polypeptide-Associated Complex (NAC). This suggests that eEF1A's client proteins may be mutually exclusive with those bound by NAC [24], supporting the idea that eEF1A could possess its own set of specific substrates.

Our findings reveal for the first time that eEF1A2 also regulates the expression of ribosomal subunits and elongation factors at a post-transcriptional level. The mRNAs encoding these proteins are characterized by a 5′ Terminal OligoPyrimidine (5′ TOP) motif [16]. mTORC1 is a protein complex that regulates several essential cellular processes, including autophagy and protein synthesis, functioning as a key nutrient and energy sensor [36]. It is also well-established that mTORC1 activation enhances the translation of 5′ TOP mRNAs [18-20, 37]. The observed increase in translation efficiency of 5′ TOP mRNAs and the elevated levels of phosphorylated ribosomal protein S6 (pRpS6), a surrogate of mTORC1 activity, support a role for mTORC1 in this regulatory mechanism. However, treatment with Rapamycin, a well-known mTORC1 inhibitor, neither affected the expression of 5′ TOP mRNAs nor global protein synthesis in our model, while it nevertheless strongly improved cardiac function and survival. Together, our data suggests that the increase of 5′ TOP mRNAs, although it might help to maintain protein synthesis in the absence of eEF1A2, does not contribute in a major way to the development of cardiomyopathy. More importantly, 5′ TOP mRNAs translation in adult cardiomyocytes is mTORC1-dependent, but rapamycin-resistant in vivo, as also previously reported by Thoreen et al. in different cultured cell types [38].

Activation of the unfolded protein response (UPR) by misfolded proteins inhibits global translation [39] through phosphorylation of eIF2α [40], in order to restore protein homeostasis [41]. Our results clearly demonstrate UPR activation, indicated by increased eIF2α phosphorylation [42], in eEF1A2-cKO cardiac tissue. However, this activation occurs without a corresponding decrease in global protein synthesis. This intriguing finding may be explained by the observed increase in ribosomal subunits and translation factors. Such compensatory upregulation could help to maintain protein synthesis even in the presence of UPR activation. The significance of the increased levels in cardiomyocytes of both phosphorylated and total eIF2α remains unknown. Of note, a recent study demonstrated that phosphorylation of Eif2α by HRI exerts a protective role in a model of mitochondrial cardiomyopathy [43]. Whether this response is ultimately protective or detrimental remains an open question that future studies will need to address.

Autophagy is a highly conserved pathway in eukaryotes and is essential for maintaining cellular homeostasis by degrading excess or damaged intracellular components [44]. There are three main types of autophagy: macroautophagy, microautophagy, and chaperone-mediated autophagy (CMA) [45]. The relationship between macroautophagy, involved in the clearance of protein aggregates and entire organelles, and cardiac dysfunction following cardiac stress is complex and, at times, contradictory. For example, Kuhn et al. [46] and Maejima et al. [47] demonstrated that overexpression of FYCO1 or Mst1, both regulators of the autophagy machinery, are essential for adaptation to cardiac stress. Similarly, Nakai et al. [48] showed that inhibition of autophagy through Atg5 deletion worsens cardiac function under stress conditions. In contrast, Zhu et al. [49] reported that constitutive overexpression of Beclin1, a key regulator of early autophagosome formation, exacerbates cardiac dysfunction following transverse aortic constriction (TAC), highlighting the delicate balance required in autophagy regulation.

The accumulation of p62-positive bodies and LC3-II in cardiomyocytes at the stage when cardiac dysfunction is evident suggests that macroautophagy is inefficient in eEF1A2-deficient hearts and plays a critical role in cardiac dysfunction. Importantly, we demonstrated that mTORC1 activation, which inhibits macroautophagy (reviewed in [50]), is a key driver of this phenotype, as rapamycin, a specific mTORC1 inhibitor, restores macroautophagy activity and improves cardiac function in eEF1A2-deficient hearts. Our results further support the concept that autophagy plays a critical role in maintaining cardiac function and, importantly, that alterations in autophagy represent a shared pathogenic mechanism across different genetic models of cardiac dysfunction. Despite the clear relationship between eEF1A2, mTORC1 activation, and impaired macroautophagy, the precise

molecular mechanism remains unknown. Based on our findings, we propose two possible non-mutually exclusive scenarios. In the first, the absence of eEF1A2 directly activates cardiac mTORC1, leading to a subsequent reduction in autophagy activity and subsequent accumulation of autophagosomes and misfolded proteins [51]. How the lack of eEF1A2 leads to increased mTORC1 activation remains unclear, but it might involve sensing increased nutrient availability due to increased levels of aminoacyl-tRNAs or alternatively promoting the assembly of the mTORC1 complex. A previous study from Qian et al.[52] demonstrated that intracellular chaperones act as inhibitors of mTOR complex assembly and showed that partial downregulation of Hsp90 was sufficient to activate mTORC1. Here, we demonstrate that eEF1A2 acts as a chaperone-like protein in cardiomyocytes and may function similarly to Hsp90 in regulating mTORC1 activity. Notably, we observed increased expression of Atg7 and Beclin1, two key activators of autophagosome formation, along with an accumulation of autophagosomes but a lack of autolysosomes in eEF1A2-cKO mice. Together, these findings suggest a defect in autophagosome–lysosome fusion in this model. In the second scenario, the accumulation of phagosomes containing unfolded proteins sequesters lysosomes away from autophagosomes. This hypothesis is supported by the high degree of colocalization between p62 and protein aggregates within the same cardiomyocytes. In this context, rapamycin may reduce unfolded protein accumulation either directly or indirectly by increasing the fidelity of protein translation, as previously demonstrated [53].

Among our main findings are the positive effects of Rapamycin administration on cardiomyopathy in eEF1A2-cKO mice. Rapamycin and its derivatives, which are FDA-approved drugs, are currently used as immunosuppressants to prevent organ rejection after transplantation and to reduce re-stenosis in vessels. Our study expands the spectrum of cardiac disease models in which Rapamycin exerts therapeutic benefits. Previous studies, such as those by Choi et al. and Ramos et al. [54, 55], have shown that Rapamycin and its derivatives prevent cardiomyopathy in laminopathies. Moreover, Rapamycin administration has been reported to prevent or reverse cardiac dysfunction following transverse aortic constriction (TAC) in mice [56, 57]. In addition, Rapamycin increases lifespan and delays age-related dysfunction in different organism such as rodents [58-62] and flies [53]. Here, we demonstrated that administration of Rapamycin in the early stage of eEF1A2-cKO cardiomyopathy reverses systolic dysfunction, cardiac hypertrophy and enhances autophagic flux, but more importantly, improves mouse survival. Notably, however, Rapamycin did not reverse fibrosis. This observation is consistent with previous findings in Lamin A/C–mediated cardiomyopathies, where Rapamycin restored cardiac function, but did not reduce fibrosis [54]. Nevertheless, although it might seem initially counterintuitive to treat cardiomyopathy caused by lack of a canonical translation elongation factor with an mTORC1 inhibitor, which could also result in reduced protein synthesis, we show its therapeutic effectiveness at the early disease stages mainly by enhancing autophagic flux, while not effecting overall protein synthesis activity. Our endpoint was two months after EEF1A2 deletion. Our data clearly show short-term benefits on cardiac function and survival, but its long-term effects remain uncertain. Future experiment will address this important question, in order to develop Rapamycin treatment for the use as tailored treatment option in patients suffering from cardiomyopathy due to mutations in the EEF1A2 gene.

Our study focused on the cardiac-specific role of eEF1A2. As previously reported, eEF1A2 is also highly expressed in neurons, and mutations in this gene are besides cardiomyopathy associated with intellectual disability, intractable epilepsy, and, in some cases, autism in patients. It would be of great interest to investigate whether some of these patient-derived eEF1A2 mutations also impair proteostasis, and, more importantly, whether Rapamycin or its derivatives could have therapeutic potential in this context.

In summary, we characterized for the first time the role of eEF1a2 as a critical mediator of cardiac proteostasis, independent of its canonical role in protein synthesis. Mechanistically, we demonstrated that eEF1A2 deficiency impairs cardiac function by reducing both autophagy activity and protein folding capacity. More importantly, we showed that mTORC1 signaling plays a central role in this process. Treatment with rapamycin, an mTORC1 inhibitor, effectively restored cardiac proteostasis and function in eEF1A2-cKO hearts.

Material and Methods

Animal studies

All animal experiments were performed according to the regulations issued by the Committee for Animal Rights Protection of the State of Baden-Württemberg (Regierungspraesidium Karlsruhe, experimental protocol G-92/20).

Mouse lines

The *Eef1a1* and *Eef1a2* conditional knockout mouse lines were generated by Cyagen Biosciences (Santa Clara, CA, USA). *Eef1a1* and *Eef1a2* conditional knock-out mouse lines were generated by flanking exons 2–8 (Eef1a1 flox/flox) or exons 2–5 (Eef1a2 flox/flox) with loxP sites. Floxed mice were crossed with heterozygous αMHC–MerCreMer transgenic mice to obtain cardiomyocyte-specific, tamoxifen-inducible gene deletion. For double *Eef1a1* and *Eef1a2* conditional knockout mice, we first generated Eef1a1 flox/flox; Eef1a2 flox/flox mice, which were the crossed with αMHC–MerCreMer +/- transgenic mice to obtain cardiomyocyte-specific, tamoxifen-inducible gene deletion.

Male and female mice were used in all experiments, except for Ribo-Seq and polysome profiling, where only male mice were used to reduce variability. At least three independent cohorts (derived from different breeding pairs) were used for all in vivo experiments and for experiments using isolated cardiomyocytes.

Tamoxifen injection

A stock solution of tamoxifen (8 mg/mL) was prepared in Miglyol® 812 (Caesar & Loretz GmbH, Hilden, Germany) and heated to 56 °C until completely dissolved. Mice aged 6–7 weeks received tamoxifen at a dose of 40 µg/g body weight via daily intraperitoneal injections for five consecutive days.

Rapamycin administration

A stock solution of rapamycin was prepared at 1.5 mg/mL in a vehicle containing 5% Tween 80 (Sigma) and 5% PEG-400 (Sigma), sterile-filtered, and stored as single-use aliquots at −80 °C, as previously described [55]. Vehicle control solutions were prepared identically but without rapamycin. Rapamycin was administered daily by intraperitoneal injection at a dose of 8 mg/kg body weight (5.33 µL/g body weight). Mice were weighed weekly, and euthanasia was performed 24 hours after the final injection.

Transthoracic echocardiography

Echocardiography was performed under 1% isoflurane anesthesia. Mice were placed in the supine position on a heated platform to maintain body temperature, while ECG and respiratory rate were continuously monitored. Transthoracic echocardiography was performed using a 30–40 MHz linear transducer (MX-550D) with a Vevo 3100 imaging system (VisualSonics, Toronto, Canada). Data were analyzed using Vevo Lab software (v5.5.0). All echocardiographic analyses were performed in a blinded manner, with the operator unaware of mouse genotype and treatment. Parameters were recorded in

B-mode and M-mode in both parasternal long-axis (PSLAX) and short-axis view at the papillary muscle level. Left-ventricular posterior wall thickness and left-ventricular end-diastolic volume were used to characterize LV microanatomy and the change of LV diameter length from end-diastole to end-systole was used to assess contractility and to calculate LV ejection fraction and fractional shortening, which were measured with the PSLAX mode in the analysis.

Organ harvest

At the end of the experiment, mice were weighed and euthanized by cervical dislocation to collect different organs. Organs were washed in cold PBS to remove the blood, and additionally the heart was washed in 0.5% (w/v) KCl in PBS. The heart was transversely cut into half, and the upper half was immediately embedded in optimal cutting temperature (OCT) compound for histological analysis, while the left ventricle from the remaining half was dissected and snap-frozen in liquid nitrogen.

For ribosome profiling (Ribo-Seq) experiments, mice were perfused through the apex of the left ventricle with cycloheximide (CHX) in PBS. The entire left ventricle was then isolated in ice-cold CHX–PBS and immediately snap-frozen in liquid nitrogen.

RNA isolation and quantitative PCR

For mRNA isolation, cardiac tissue or cultured cells were homogenized in 1 mL TRIzol reagent. Cardiac tissue was homogenized using a TissueLyser II (Qiagen) for 2 minutes at 20 Hz. Following centrifugation at 12,500 × g for 10 minutes at 4 °C, 200 µL chloroform was added, and samples were incubated for 10 minutes at room temperature. Samples were then centrifuged at 12,000 × g for 15 minutes at 4 °C, and the aqueous phase was collected. RNA was precipitated by adding 500 µL isopropanol and incubating for 30 minutes on ice, followed by purification using NucleoSpin RNA columns (Macherey-Nagel) according to the manufacturer's instructions.

cDNA was synthesized using the Maxima H Minus First Strand cDNA Synthesis Kit (Thermo Fisher Scientific, K1652). Quantitative PCR (qPCR) was performed using PowerUp™ SYBR™ Green Master Mix with ROX as a reference dye (Thermo Fisher Scientific, A25742) on an AriaMx Real-Time PCR System (Agilent, G8830A). All qRT-PCR primer sequences are listed in Supplemental Table S1.

Protein isolation

For protein extraction, cardiac tissue or cells were lysed in sampling buffer (30 µL/mg tissue) containing 50 mM Tris-HCl (pH 6.7), 2% SDS, 10% glycerol, a protease inhibitor cocktail (Roche), and phosphatase inhibitor cocktail set V (Millipore). Lysates were centrifuged at 12,500 × g for 15 minutes, and protein concentrations were determined using a BCA assay (Pierce). Samples were then incubated at 95 °C for 5 minutes after addition of Laemmli buffer (1× final concentration). Proteins were either stored at −20 °C or separated by SDS–PAGE. All antibodies and their dilutions are listed in Supplemental Table S2.

Histology

OCT-embedded organs were sectioned using a cryostat at a thickness of 7 µm for immunofluorescence and 12 µm for Picrosirius red staining. For immunofluorescence, tissue sections were fixed in 4% paraformaldehyde (PFA), permeabilized with 0.3% Triton X-100 in PBS, and blocked with 3% BSA. Primary and secondary antibodies used in this study are listed in Supplemental Table S2. Samples were visualized using a Leica SP8 confocal microscope (Leica Microsystems, Wetzlar, Germany), and images were analyzed using Leica Application Suite X (LAS X) software version 3.7.

Picrosirius red staining was performed by fixing tissue sections in 100% ice-cold acetone, followed by staining according to a standard protocol. Tissue sections were scanned using a Zeiss Axio Scan.Z1

system (Carl Zeiss Microscopy GmbH, Jena, Germany), and images were analyzed using ZEN 2.6 Blue Edition software (Carl Zeiss Microscopy GmbH, Jena, Germany).

PROTEOSTAT staining of cardiac tissue

Tissue sections were fixed in 3.7% methanol-free formaldehyde (Pierce) diluted in 1× assay buffer for 30 minutes at room temperature, washed twice with phosphate-buffered saline (PBS), and permeabilized with 0.5% Triton X-100 in 1× assay buffer for 30 minutes. After two additional washes, sections were incubated with PROTEOSTAT® Aggresome Detection Reagent (Enzo Life Sciences), diluted in assay buffer according to the manufacturer's instructions, for 30 minutes at room temperature in the dark. Sections were then washed twice and blocked with 3% BSA in PBS for 1 hour at room temperature, followed by incubation with primary antibodies diluted in 3% BSA in PBS overnight at 4 °C. The following day, sections were incubated with the appropriate secondary antibodies for 1 hour at room temperature. Finally, sections were mounted with VECTASHIELD HardSet Antifade Mounting Medium containing DAPI (Vector Laboratories) and sealed with nail polish.

Adenovirus generation and infection

Adenoviral vectors were used to overexpress standard, STOP, and R218S firefly luciferase together with Renilla luciferase. To eliminate a PacI restriction site while preserving the original amino acid sequence, a silent mutation was introduced at leucine 440 of firefly luciferase (TTA→TTG) in the original plasmid (kindly provided by Dr. Xie, [26]). The modified luciferase sequences were subcloned into the promoterless pShuttle vector (Addgene plasmid #16402), and recombinant adenoviruses were generated using the AdEasy Adenoviral Vector System (Agilent Technologies, Waldbronn, Germany) in AD-293 cells (Agilent) according to the manufacturer's instructions. Viral titers were determined using the AdEasy Viral Titer Kit (Agilent Technologies). For adenoviral infection, cardiomyocytes were maintained in medium containing heat-inactivated fetal calf serum. Three hours after isolation, cells were infected overnight at a multiplicity of infection (MOI) of 100.

Luciferase assay

100 000 isolated cardiomyocytes were plated per well (of a 6 well-plate) treated with laminin A (Santa Cruz). After 3 hours, cells were infected overnight at a multiplicity of infection (MOI) of 100. The next day, the medium was replaced with fresh culture medium. Luciferase activity (Firefly and Renilla) was measured after 48 hours post infection using the Dual-Luciferase® Reporter Assay System (Promega) according to the manufacturer's instructions. For each isolation, signals from non-infected cardiomyocytes were used as background. Luciferase activity was calculated by subtracting the background from each sample.

Electron microscopy

Immediately after cervical dislocation, hearts were perfused with freshly prepared Perfixol solution containing 24 mM cacodylic acid (Sigma, Cat. No. 20835), 4% paraformaldehyde, and 2.5% glutaraldehyde (Sigma, Cat. No. 354400), pH 7.2. The left ventricle was then dissected and cut into small squares, which were incubated overnight at 4 °C in Perfixol. After rinsing in buffer, the samples were further fixed in 1% osmium in 0.1M cacodylate buffer for 1h at room temperature, washed in water, and incubated in 1% uranylacetate in water overnight at 4˚C. Dehydration was done in 10 min steps in an acetone gradient followed by stepwise Spurr resin infiltration at room temperature and polymerization at 60˚C. The blocks were sectioned using a Leica UC6 ultramicrotome (Leica Microsystems Vienna) in 70nm thin sections and placed on formvar coated slot grids, post-stained with 3% uranyl acetate in water and Reynold's lead citrate and imaged on a JEOL JEM-1400 electron

microscope (JEOL, Tokyo) operating at 80 kV and equipped with a 4K TemCam F416 (Tietz Video and Image Processing Systems GmBH, Gautig).

Ribo-seq analysis

Left ventricular tissue was homogenized in 500 µL ice-cold polysome buffer (20 mM Tris-HCl, pH 7.4, 10 mM $MgCl_2$, 200 mM KCl, 2 mM DTT, 1% Triton X-100, 1 U DNase/µL) supplemented with 100 µg/mL cycloheximide using a tissue homogenizer. Following complete lysis, 200 µL of polysome buffer was added, and lysates were passed six times through a 23-gauge needle. Samples were centrifuged at 20,000 × g for 15 min at 4°C, and the supernatant was immediately processed. An aliquot (100 µL) was reserved for total RNA extraction using TRIzol, while ribosomal footprints were isolated from the remaining lysate using MicroSpin™ S-400 HR columns (Merck) according to the manufacturer's instructions. SDS (10%, 10 µL per 100 µL eluate) was added, and RNA was purified using the RNA Clean & Concentrator-25 kit (Zymo Research).

Total RNA (5 µg) was subjected to rRNA depletion using the RiboPool Kit (Biozym) and precipitated with GlycoBlue, NaCl, and isopropanol. Fragmentation was performed by incubating RNA in 2× fragmentation buffer (2 mM EDTA, 85 mM $NaHCO_3$, 120 mM Na_2CO_3) at 95°C for 12 min. Fragmented RNA was size-selected (25–35 nt) by 15% TBE–urea PAGE, visualized with SYBR Gold (Invitrogen), and gel slices were eluted overnight at 4°C in 0.3 M NaCl containing RNaseOUT. RNA was recovered by filtration and isopropanol precipitation. End repair was performed using T4 polynucleotide kinase (NEB) at 37°C for 1 h, followed by RNA precipitation and resuspension in RNase-free water.

Small RNA libraries were prepared using the NEXTflex Small RNA-Seq Kit v3 (PerkinElmer) with pre–size-selected RNA. Adapter-ligated libraries were amplified using a qPCR-determined number of cycles to avoid overamplification. Library quality and size distribution were assessed using a Bioanalyzer High Sensitivity DNA kit (Agilent). Sequencing was performed on an Illumina NextSeq 550 using the NextSeq 500/550 High Output Kit v2.5 (75 cycles).

Raw reads from four WT, four eEF1A2-cKO, and four eEF1A1/eEF1A2-cKO biological replicates were processed by trimming adapters with Cutadapt and removing rRNA/tRNA-mapping reads using Bowtie2. Remaining reads were aligned to the mouse reference genome (Ensembl release 98) using STAR v2.7.3a, retaining only uniquely mapped reads. Quality control and P-site assignment were performed using Ribo-seQC. All samples exhibited robust three-nucleotide periodicity (81–84%), with predominant read lengths of 28–29 nt. P-sites overlapping annotated coding sequences were quantified to calculate codon frequencies, and relative usage differences between genotypes were determined.

RNA-seq and bioinformatics

RNA isolation was performed from isolated left ventricles as described at the indicated time points (1 or 2 months post tamoxifen injection). Quality control of RNA samples (Agilent 2100 Fragment Analyzer) and library preparation (DNBSEQ Eukaryotic Strand-specific mRNA library) were performed by BGI, Hong Kong. Bulk RNA-seq from different samples was performed as stranded and single-end with 50-base sequence read length by BGI with an Illumina HiSeq 2500. Initially, the trimming of adapter sequences from fastq files was performed with the R package FastqCleaner. For aligning the reads to the reference genome (mm10) after trimming, the R package bowtie2 alignment tool was used. Gene annotation was performed with the bioMaRt R package. Library size of the samples was normalized to counts per million (cpm) and transformed into log2 values followed by calculation of differential gene expression with the edgeR package of R. Significant changes in gene expression between compared groups were filtered based on FDR < 0.05 and fold change > 1.0. Gene ontology analysis was performed with Metascape and DAVID online tools.

Ribosome profiling

Tissue isolation for polysome profiling: Quickly after the euthanization of the mice, hearts were perfused with a solution containing PBS and cycloheximide (150 µg/ml), for stalling the ribosomes in the tissue. Next, the heart was removed and washed in PBS/CHX solution to remove the remaining blood, and snap frozen in liquid nitrogen and stored at – 80°C.

Tissue lysis for polysome profiling

The left isolated left ventricle was lysed in 900 µL ice-cold polysome buffer without Triton X-100 (20 mM Tris-HCl, pH 7.4, 10 mM $MgCl_2$, 200 mM KCl, 2 mM DTT, 1 U DNase/µL) supplemented with 100 µg/mL cycloheximide using the TissueLyser II (Qiagen) for 2 minutes at 200 Hertz. Next, Triton X-100 was added to the sample to reach 1% and the sample were incubated for 30 minutes at 4 °C in an endless end to end rotor followed by a centrifugation at 17,000 g for 6 minutes at 4 °C. The supernatant was collected and centrifuged again as before.

Polysome fractionation and profiling

250 µl of lysate per gradient was loaded on a sucrose gradients (17.5 % - 50 %) and centrifuged for 2 h (40 000 rpm at 4°C) in a SW60 rotor (Acceleration: 7, Deceleration: 1). Next, gradients were eluted with a Teledyne Isco Foxy Jr. system into 16 fractions of similar volume and the optical density of the fractions was measured.

mRNA and protein isolation

Half of the volume of each fraction was used for mRNA isolation whereas the other half was used by protein isolation. For mRNA isolation, to each fraction a 1 mL of Trizol was added and the mRNA was isolated as previously described. For protein isolation we used the same method as previously described by Poetz et al [63].

Isolation and cultured of adult cardiomyocytes

Isolation and culture of adult mice cardiomyocytes were done as previously described by Acker-Johnson et al. [64] with the minor differences suggested by Callagham et al [65].

Generation of stable overexpressing Eef1a2 HEK lines

Mouse Eef1a2 was cloned and inserted in pAAVS1-Nst-MCS. Next, AD-293 cells were transfected with pAAVS1-Nst-Eef1a2 [66] and pX459-HypaCas9-AAVS1_sgRNA [67]. 48 hours later, transfected cells were selected by puromycin incubation for 72 hours and single cells were growth. Two different single clones that overexpressed Eef1a2 were selected. Two single clones without-Eef1a2 overexpression as well as parental cells were used as control.

Luciferase unfolding and refolding assay

AD-293 cells parental cells, as well as clones overexpressing Eef1a2 and non-targeting Eef1a2 control clones, were transfected with the plasmid described in the Adenovirus section using Lipofectamine 3000 (Invitrogen). The following day, cells were split and seeded at a density of 9×10^5 cells per well. On the next day, cycloheximide (CHX; final concentration 20 µg/mL) and MOPS buffer (pH 7.0; final concentration 20 mM) were added to the culture medium and incubated for 30 minutes. Cells were then subjected to heat shock at 43 °C for 1 hour or maintained at 37 °C as a control. After heat shock, cells were allowed to recover at 37 °C for either 1 hour or 3 hours. At the indicated time points, cells were lysed with 400 µL of 1× Passive Lysis Buffer (Promega), and Firefly and Renilla luciferase activities were measured using the Dual-Luciferase® Reporter Assay System (Promega).

Proteomic analysis

Sample preparation, mass spectrometry, and proteomic analyses were performed as previously described [68]. Proteins were classified as hits if they met a false discovery rate (FDR) < 5% and exhibited a fold change ≥ 100%, and as candidates if they met an FDR < 20% with a fold change ≥ 50%.

Only proteins identified as hit or candidates were included in the analysis. Pathway enrichment analysis was performed using the Metascape online platform.

Schematic representations

Schematic representations were prepared with Biorender software.

Statistical analysis

All statistical analysis was performed using GraphPad Prism 8. Graphs are presented as mean ± SD. Each statistical test is also included in the respective figure legend. P values less than 0.05 were considered statistically significant.

Acknowledgement

The authors are grateful to the Core Facilities Pre-Clinical Models and Live Cell Imaging Mannheim (LIMA), as well as for the support provided by the Electron Microscopy Core Facility (EMCF; RI_00565) at Heidelberg University. We also acknowledge the EMBL Proteomics Core Facility for conducting the proteomics analysis and Eva Rog-Zielinska, PhD, for her expert analysis and interpretation of electron microscopy images.

Author contributions

A. M.-G. designed and performed most of the experiments, analyzed data and wrote the first draft of the manuscript. N.W., J.E., S.R., V.S., A.G., M.K., N.W., E.H., F.A.T., S.H. performed experiments. J. R.-O. and J.C. analyzed data. G.S., M.V., N. H. and G.D. supervised experiments and critically revised the manuscript. J.H. designed and conceptualized the study, supervised experiments and prepared the final draft of the manuscript. All authors read and approved the manuscript.

Sources of Funding

This study was supported by SFB1550-project ID464424253: Collaborative Research Center 1550 (CRC1550) “Molecular Circuits of Heart Disease” project B01 (to J.H.) by the Deutsche Forschungsgemeinschaft.

Disclosures

None.

References

1. Kahns, S., et al., *The elongation factor 1 A-2 isoform from rabbit: cloning of the cDNA and characterization of the protein.* Nucleic Acids Res, 1998. **26**(8): p. 1884-90.
2. Motorin Yu, A., et al., *Mammalian valyl-tRNA synthetase forms a complex with the first elongation factor.* FEBS Lett, 1988. **238**(2): p. 262-4.
3. Slobin, L.I., *The role of eucaryotic factor Tu in protein synthesis. The measurement of the elongation factor Tu content of rabbit reticulocytes and other mammalian cells by a sensitive radioimmunoassay.* Eur J Biochem, 1980. **110**(2): p. 555-63.

4. Newbery, H.J., et al., *Translation elongation factor eEF1A2 is essential for post-weaning survival in mice.* J Biol Chem, 2007. **282**(39): p. 28951-28959.
5. Chambers, D.M., J. Peters, and C.M. Abbott, *The lethal mutation of the mouse wasted (wst) is a deletion that abolishes expression of a tissue-specific isoform of translation elongation factor 1alpha, encoded by the Eef1a2 gene.* Proc Natl Acad Sci U S A, 1998. **95**(8): p. 4463-8.
6. Petroulakis, E. and E. Wang, *Nerve growth factor specifically stimulates translation of eukaryotic elongation factor 1A-1 (eEF1A-1) mRNA by recruitment to polyribosomes in PC12 cells.* J Biol Chem, 2002. **277**(21): p. 18718-27.
7. Feng, W., et al., *Loss of eEF1A2 (Eukaryotic Elongation Factor 1 A2) in Murine Myocardium Results in Dilated Cardiomyopathy.* Circ Heart Fail, 2021. **14**(10): p. e008665.
8. Mateyak, M.K. and T.G. Kinzy, *eEF1A: thinking outside the ribosome.* J Biol Chem, 2010. **285**(28): p. 21209-13.
9. Ruiz-Orera, J., et al., *Evolution of translational control and the emergence of genes and open reading frames in human and non-human primate hearts.* Nat Cardiovasc Res, 2024. **3**(10): p. 1217-1235.
10. Cao, S., et al., *Homozygous EEF1A2 mutation causes dilated cardiomyopathy, failure to thrive, global developmental delay, epilepsy and early death.* Hum Mol Genet, 2017. **26**(18): p. 3545-3552.
11. Lewis, Y.E., et al., *Localization of transcripts, translation, and degradation for spatiotemporal sarcomere maintenance.* J Mol Cell Cardiol, 2018. **116**: p. 16-28.
12. Haddad, R., et al., *Localized translation and sarcomere maintenance requires ribosomal protein SA in mice.* J Clin Invest, 2024. **134**(13).
13. Scarborough, E.A., et al., *Microtubules orchestrate local translation to enable cardiac growth.* Nat Commun, 2021. **12**(1): p. 1547.
14. Sinha, N.K., et al., *EDF1 coordinates cellular responses to ribosome collisions.* Elife, 2020. **9**.
15. Juszkiewicz, S., et al., *Ribosome collisions trigger cis-acting feedback inhibition of translation initiation.* Elife, 2020. **9**.
16. Avni, D., et al., *Vertebrate mRNAs with a 5'-terminal pyrimidine tract are candidates for translational repression in quiescent cells: characterization of the translational cis-regulatory element.* Mol Cell Biol, 1994. **14**(6): p. 3822-33.
17. Tang, H., et al., *Amino acid-induced translation of TOP mRNAs is fully dependent on phosphatidylinositol 3-kinase-mediated signaling, is partially inhibited by rapamycin, and is independent of S6K1 and rpS6 phosphorylation.* Mol Cell Biol, 2001. **21**(24): p. 8671-83.
18. Jefferies, H.B., et al., *Rapamycin selectively represses translation of the "polypyrimidine tract" mRNA family.* Proc Natl Acad Sci U S A, 1994. **91**(10): p. 4441-5.
19. Fonseca, B.D., et al., *La-related Protein 1 (LARP1) Represses Terminal Oligopyrimidine (TOP) mRNA Translation Downstream of mTOR Complex 1 (mTORC1).* J Biol Chem, 2015. **290**(26): p. 15996-6020.
20. Thoreen, C.C., et al., *A unifying model for mTORC1-mediated regulation of mRNA translation.* Nature, 2012. **485**(7396): p. 109-13.
21. Saxton, R.A. and D.M. Sabatini, *mTOR Signaling in Growth, Metabolism, and Disease (vol 168, pg 960, 2017).* Cell, 2017. **169**(2): p. 362-362.
22. Dikic, I. and Z. Elazar, *Mechanism and medical implications of mammalian autophagy.* Nature Reviews Molecular Cell Biology, 2018. **19**(6): p. 349-364.
23. Lukash, T.O., et al., *Chaperone-like activity of mammalian elongation factor eEF1A: renaturation of aminoacyl-tRNA synthetases.* Int J Biochem Cell Biol, 2004. **36**(7): p. 1341-7.
24. Hotokezaka, Y., et al., *Interaction of the eukaryotic elongation factor 1A with newly synthesized polypeptides.* J Biol Chem, 2002. **277**(21): p. 18545-51.
25. Suzuki, H., et al., *Chaperone properties of mammalian mitochondrial translation elongation factor Tu.* J Biol Chem, 2007. **282**(6): p. 4076-84.
26. Xie, J., et al., *Regulation of the Elongation Phase of Protein Synthesis Enhances Translation Accuracy and Modulates Lifespan.* Curr Biol, 2019. **29**(5): p. 737-749 e5.

27. Carr-Schmid, A., et al., *Mutations in a GTP-binding motif of eukaryotic elongation factor 1A reduce both translational fidelity and the requirement for nucleotide exchange.* J Biol Chem, 1999. **274**(42): p. 30297-302.
28. Pape, T., W. Wintermeyer, and M. Rodnina, *Induced fit in initial selection and proofreading of aminoacyl-tRNA on the ribosome.* EMBO J, 1999. **18**(13): p. 3800-7.
29. Chorghade, S., et al., *Poly(A) tail length regulates PABPC1 expression to tune translation in the heart.* Elife, 2017. **6**.
30. Chuang, S.M., et al., *Proteasome-mediated degradation of cotranslationally damaged proteins involves translation elongation factor 1A.* Molecular and Cellular Biology, 2005. **25**(1): p. 403-413.
31. Meriin, A.B., N. Zaarur, and M.Y. Sherman, *Association of translation factor eEF1A with defective ribosomal products generates a signal for aggresome formation.* Journal of Cell Science, 2012. **125**(11): p. 2665-2674.
32. Vera, M., et al., *The translation elongation factor eEF1A1 couples transcription to translation during heat shock response.* Elife, 2014. **3**: p. e03164.
33. Kudlicki, W., et al., *Renaturation of rhodanese by translational elongation factor (EF) Tu. Protein refolding by EF-Tu flexing.* J Biol Chem, 1997. **272**(51): p. 32206-10.
34. Caldas, T.D., A. El Yaagoubi, and G. Richarme, *Chaperone properties of bacterial elongation factor EF-Tu.* J Biol Chem, 1998. **273**(19): p. 11478-82.
35. Ranek, M.J., et al., *The role of heat shock proteins and co-chaperones in heart failure.* Philos Trans R Soc Lond B Biol Sci, 2018. **373**(1738).
36. Ma, X.M. and J. Blenis, *Molecular mechanisms of mTOR-mediated translational control.* Nat Rev Mol Cell Biol, 2009. **10**(5): p. 307-18.
37. Jia, J.J., et al., *mTORC1 promotes TOP mRNA translation through site-specific phosphorylation of LARP1.* Nucleic Acids Res, 2021. **49**(6): p. 3461-3489.
38. Thoreen, C.C., et al., *An ATP-competitive mammalian target of rapamycin inhibitor reveals rapamycin-resistant functions of mTORC1.* J Biol Chem, 2009. **284**(12): p. 8023-32.
39. Colthurst, D.R., D.G. Campbell, and C.G. Proud, *Structure and regulation of eukaryotic initiation factor eIF-2. Sequence of the site in the alpha subunit phosphorylated by the haem-controlled repressor and by the double-stranded RNA-activated inhibitor.* Eur J Biochem, 1987. **166**(2): p. 357-63.
40. Gordiyenko, Y., J.L. Llacer, and V. Ramakrishnan, *Structural basis for the inhibition of translation through eIF2alpha phosphorylation.* Nat Commun, 2019. **10**(1): p. 2640.
41. Hetz, C., K. Zhang, and R.J. Kaufman, *Mechanisms, regulation and functions of the unfolded protein response.* Nat Rev Mol Cell Biol, 2020. **21**(8): p. 421-438.
42. Dever, T.E., et al., *Phosphorylation of initiation factor 2 alpha by protein kinase GCN2 mediates gene-specific translational control of GCN4 in yeast.* Cell, 1992. **68**(3): p. 585-96.
43. Zhu, S., et al., *Mitochondrial Stress Induces an HRI-eIF2alpha Pathway Protective for Cardiomyopathy.* Circulation, 2022. **146**(13): p. 1028-1031.
44. Miyamoto, S., *Autophagy and cardiac aging.* Cell Death Differ, 2019. **26**(4): p. 653-664.
45. Scrivo, A., et al., *Selective autophagy as a potential therapeutic target for neurodegenerative disorders.* Lancet Neurol, 2018. **17**(9): p. 802-815.
46. Kuhn, C., et al., *FYCO1 Regulates Cardiomyocyte Autophagy and Prevents Heart Failure Due to Pressure Overload In Vivo.* JACC Basic Transl Sci, 2021. **6**(4): p. 365-380.
47. Maejima, Y., et al., *Mst1 inhibits autophagy by promoting the interaction between Beclin1 and Bcl-2.* Nat Med, 2013. **19**(11): p. 1478-88.
48. Nakai, A., et al., *The role of autophagy in cardiomyocytes in the basal state and in response to hemodynamic stress.* Nat Med, 2007. **13**(5): p. 619-24.
49. Zhu, H., et al., *Cardiac autophagy is a maladaptive response to hemodynamic stress.* J Clin Invest, 2007. **117**(7): p. 1782-93.
50. Liu, G.Y. and D.M. Sabatini, *mTOR at the nexus of nutrition, growth, ageing and disease (vol 29, pg 145, 2020).* Nature Reviews Molecular Cell Biology, 2020. **21**(4): p. 246-246.

51. Castets, P., et al., *Sustained activation of mTORC1 in skeletal muscle inhibits constitutive and starvation-induced autophagy and causes a severe, late-onset myopathy.* Cell Metab, 2013. **17**(5): p. 731-44.
52. Qian, S.B., et al., *mTORC1 links protein quality and quantity control by sensing chaperone availability.* J Biol Chem, 2010. **285**(35): p. 27385-27395.
53. Martinez-Miguel, V.E., et al., *Increased fidelity of protein synthesis extends lifespan.* Cell Metabolism, 2021. **33**(11): p. 2288-+.
54. Choi, J.C., et al., *Temsirolimus activates autophagy and ameliorates cardiomyopathy caused by lamin A/C gene mutation.* Sci Transl Med, 2012. **4**(144): p. 144ra102.
55. Ramos, F.J., et al., *Rapamycin reverses elevated mTORC1 signaling in lamin A/C-deficient mice, rescues cardiac and skeletal muscle function, and extends survival.* Sci Transl Med, 2012. **4**(144): p. 144ra103.
56. Shioi, T., et al., *Rapamycin attenuates load-induced cardiac hypertrophy in mice.* Circulation, 2003. **107**(12): p. 1664-1670.
57. McMullen, J.R., et al., *Inhibition of mTOR signaling with rapamycin regresses established cardiac hypertrophy induced by pressure overload.* Circulation, 2004. **109**(24): p. 3050-3055.
58. Gkioni, L., et al., *The geroprotectors trametinib and rapamycin combine additively to extend mouse healthspan and lifespan.* Nature Aging, 2025. **5**(7): p. 1249-1265.
59. Harrison, D.E., et al., *Rapamycin fed late in life extends lifespan in genetically heterogeneous mice.* Nature, 2009. **460**(7253): p. 392-U108.
60. Bitto, A., et al., *Transient rapamycin treatment can increase lifespan and healthspan in middle-aged mice.* Elife, 2016. **5**.
61. Zhang, Y.Q., et al., *Rapamycin Extends Life and Health in C57BL/6 Mice.* Journals of Gerontology Series a-Biological Sciences and Medical Sciences, 2014. **69**(2): p. 119-130.
62. Neff, F., et al., *Rapamycin extends murine lifespan but has limited effects on aging.* Journal of Clinical Investigation, 2013. **123**(8): p. 3272-3291.
63. Poetz, F., et al., *RNF219 attenuates global mRNA decay through inhibition of CCR4-NOT complex-mediated deadenylation.* Nature Communications, 2021. **12**(1).
64. Ackers-Johnson, M., et al., *A Simplified, Langendorff-Free Method for Concomitant Isolation of Viable Cardiac Myocytes and Nonmyocytes From the Adult Mouse Heart.* Circ Res, 2016. **119**(8): p. 909-20.
65. Callaghan, N.I., et al., *Functional culture and in vitro genetic and small-molecule manipulation of adult mouse cardiomyocytes.* Communications Biology, 2020. **3**(1).
66. Oceguera-Yanez, F., et al., *Engineering the AAVS1 locus for consistent and scalable transgene expression in human iPSCs and their differentiated derivatives.* Methods, 2016. **101**: p. 43-55.
67. Husser, M.C., et al., *Cytokinetic diversity in mammalian cells is revealed by the characterization of endogenous anillin, Ect2 and RhoA.* Open Biology, 2022. **12**(11).
68. Wardman, R., et al., *RNA-Binding Proteins Regulate Post-Transcriptional Responses to TGF-β to Coordinate Function and Mesenchymal Activation of Murine Endothelial Cells.* Arteriosclerosis Thrombosis and Vascular Biology, 2023. **43**(10): p. 1967-1989.

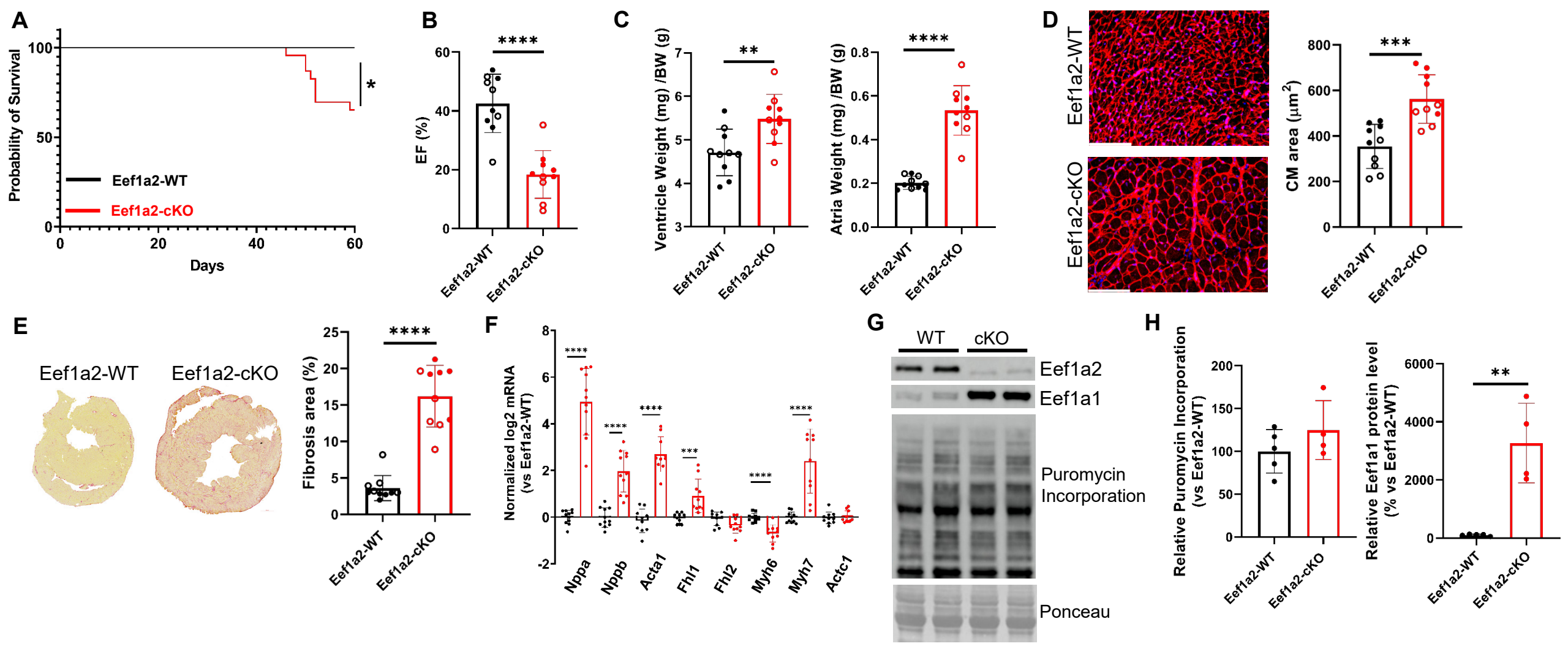
A
Probability of Survival
Days
Eef1a2-WT
Eef1a2-cKO
*
B
EF (%)
****
C
Ventricle Weight (mg) /BW (g)
**
Atria Weight (mg) /BW (g)
****
D
Eef1a2-WT
Eef1a2-cKO
CM area (μm²)
***
E
Eef1a2-WT
Eef1a2-cKO
Fibrosis area (%)
****
F
Normalized log2 mRNA (vs Eef1a2-WT)
Nppa
Nppb
Acta1
Fhl1
Fhl2
Myh6
Myh7
Actc1
G
WT
cKO
Eef1a2
Eef1a1
Puromycin Incorporation
Ponceau
H
Relative Puromycin Incorporation (vs Eef1a2-WT)
Relative Eef1a1 protein level (% vs Eef1a2-WT)
**

Figure 1. Effects of cardiomyocyte-specific Eef1a2 deletion. (A) Kaplan–Meier survival curves of Eef1a2-WT (n = 10, 10/10 survived) and Eef1a2-cKO (n = 16, 10/16 survived) mice. *P < 0.05, log-rank (Mantel–Cox) test. (**B**) Left ventricular ejection fraction of Eef1a2-WT (n = 10) and Eef1a2-cKO (n = 10) mice. ****P < 0.0001, unpaired t-test. (**C**) Ventricular (left) and atrial (right) weight normalized to body weight in Eef1a2-WT (n = 10) and Eef1a2-cKO (n = 10) mice at 2 months after Eef1a2 deletion. **P < 0.01, ****P < 0.0001; unpaired t-test. (**D**) Representative microscopic images of cardiac sections stained with wheat germ agglutinin (WGA) and corresponding quantification from Eef1a2-WT (n = 10) and Eef1a2-cKO (n = 10) mice at 2 months after Eef1a2 deletion (scale bars, 100 μm). ***P < 0.001, unpaired t-test. (**E**) Representative Sirius Red staining of cardiac fibrosis and corresponding quantification of fibrotic area from Eef1a2-WT (n = 10) and Eef1a2-cKO (n = 10) mice at 2 months after Eef1a2 deletion. ****P < 0.0001, Mann–Whitney U test. (**F)** Normalized mRNA expression levels of selected genes in cardiac tissue from Eef1a2-WT (n = 10) and Eef1a2-cKO (n = 10) mice at 2 months after Eef1a2 deletion. ***P < 0.001, ****P < 0.0001; unpaired t-test. (**G**) Representative Western blot analysis of isolated cardiomyocytes at 2 months after Eef1a2 deletion. Ponceau (Ponc.) staining shows equal protein loading and blotting. (**H**) Quantification of puromycin incorporation and Eef1a1 protein levels in isolated cardiomyocytes from Eef1a2-WT (n = 5) and Eef1a2-cKO (n = 4) mice from independent isolations at 2 months after Eef1a2 deletion. **P < 0.01; unpaired t-test. Filled circles denote males; open circles denote females.

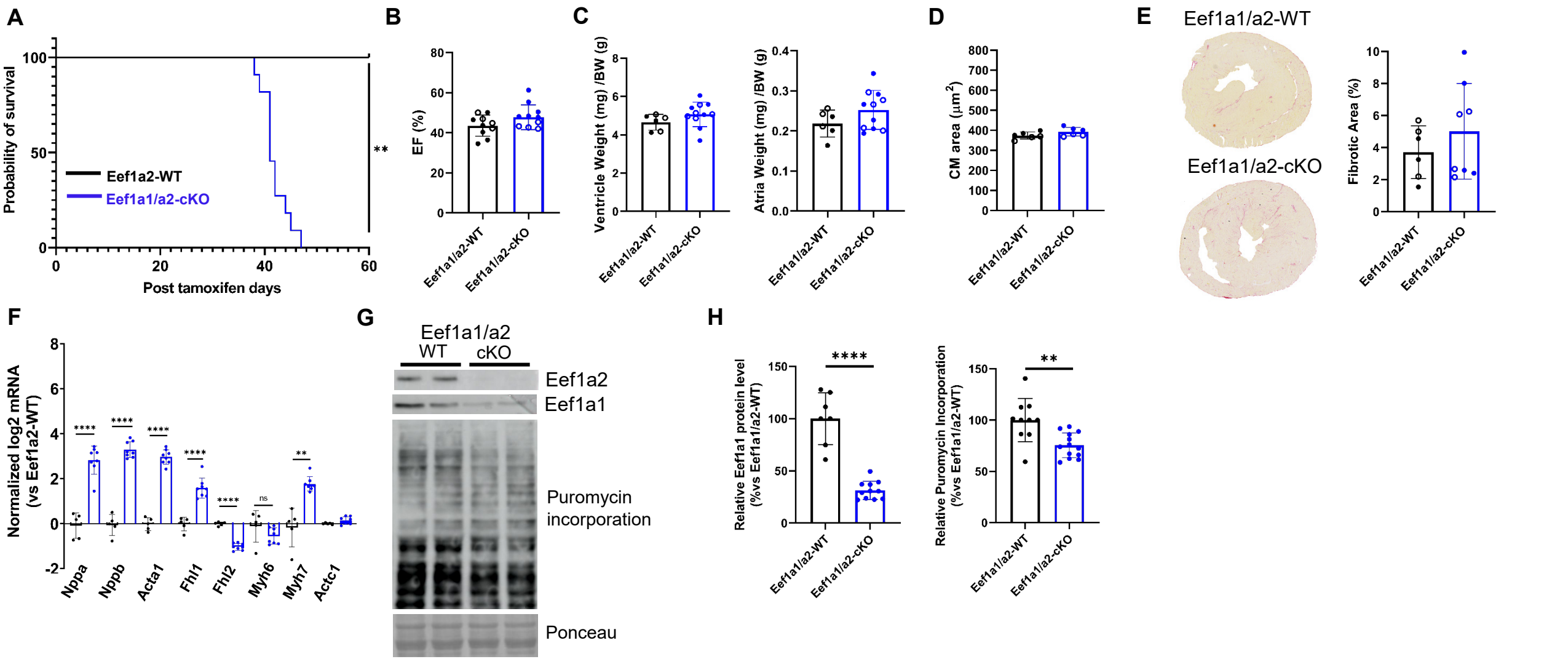
A
Probability of survival
Post tamoxifen days
Eef1a2-WT
Eef1a1/a2-cKO
**
B
EF (%)
Eef1a1/a2-WT
Eef1a1/a2-cKO
C
Ventricle Weight (mg) /BW (g)
Atria Weight (mg) /BW (g)
D
CM area (μm2)
E
Eef1a1/a2-WT
Eef1a1/a2-cKO
Fibrotic Area (%)
F
Normalized log2 mRNA (vs Eef1a2-WT)
Nppa
Nppb
Acta1
Fhl1
Fhl2
Myh6
Myh7
Actc1
****
ns
**
G
Eef1a1/a2
WT
cKO
Eef1a2
Eef1a1
Puromycin incorporation
Ponceau
H
Relative Eef1a1 protein level (%vs Eef1a1/a2-WT)
Relative Puromycin Incorporation (%vs Eef1a1/a2-WT)

Figure 2. Effects of cardiomyocyte-specific Eef1a1 and Eef1a2 deletion. (A) Kaplan–Meier survival curves of Eef1a1/a2-WT (n = 5; 5/5 survived) and Eef1a1/a2-cKO (n = 11; 0/11 survived) mice. **P < 0.01, log-rank (Mantel–Cox) test. (**B**) Left ventricular ejection fraction of Eef1a1/a2-WT (n = 10) and Eef1a1/a2-cKO (n = 11) mice at 1 month after Eef1a1/a2 deletion. (**C**) Ventricular (right) and atrial (left) weight normalized to body weight in Eef1a1/a2-WT (n = 6) and Eef1a1/a2-cKO (n = 11) mice at 1 month after Eef1a1/a2 deletion. (**D**) Quantification of cardiomyocyte cross-sectional area in Eef1a1/a2-WT (n = 6) and Eef1a1/a2-cKO (n = 6) mice at 1 month after Eef1a1/a2 deletion. (**E**) Representative Sirius Red staining of cardiac fibrosis and corresponding quantification of fibrotic area in Eef1a1/a2-WT (n = 6) and Eef1a1/a2-cKO (n = 8) mice at 1 month after Eef1a1/a2 deletion. (**F**) Normalized mRNA expression levels of selected genes in cardiac tissue from Eef1a1/a2-WT (n = 5) and Eef1a1/a2-cKO (n = 8) mice at 1 month after Eef1a1/a2 deletion. (**G**) Representative Western blot analysis of isolated cardiomyocytes at 1 month after Eef1a1/a2 deletion. Ponceau staining shows equal protein loading and blotting. (**H**) Quantification of Eef1a1 expression and puromycin incorporation in isolated cardiomyocytes from Eef1a1/a2-WT (Eef1a1, n = 7 independent isolations; puromycin, n = 10 independent isolations) and Eef1a1/a2-cKO mice (Eef1a1, n = 11; puromycin, n = 13). ****P < 0.0001, **P < 0.01; unpaired t-test. Filled circles denote males; open circles denote females.

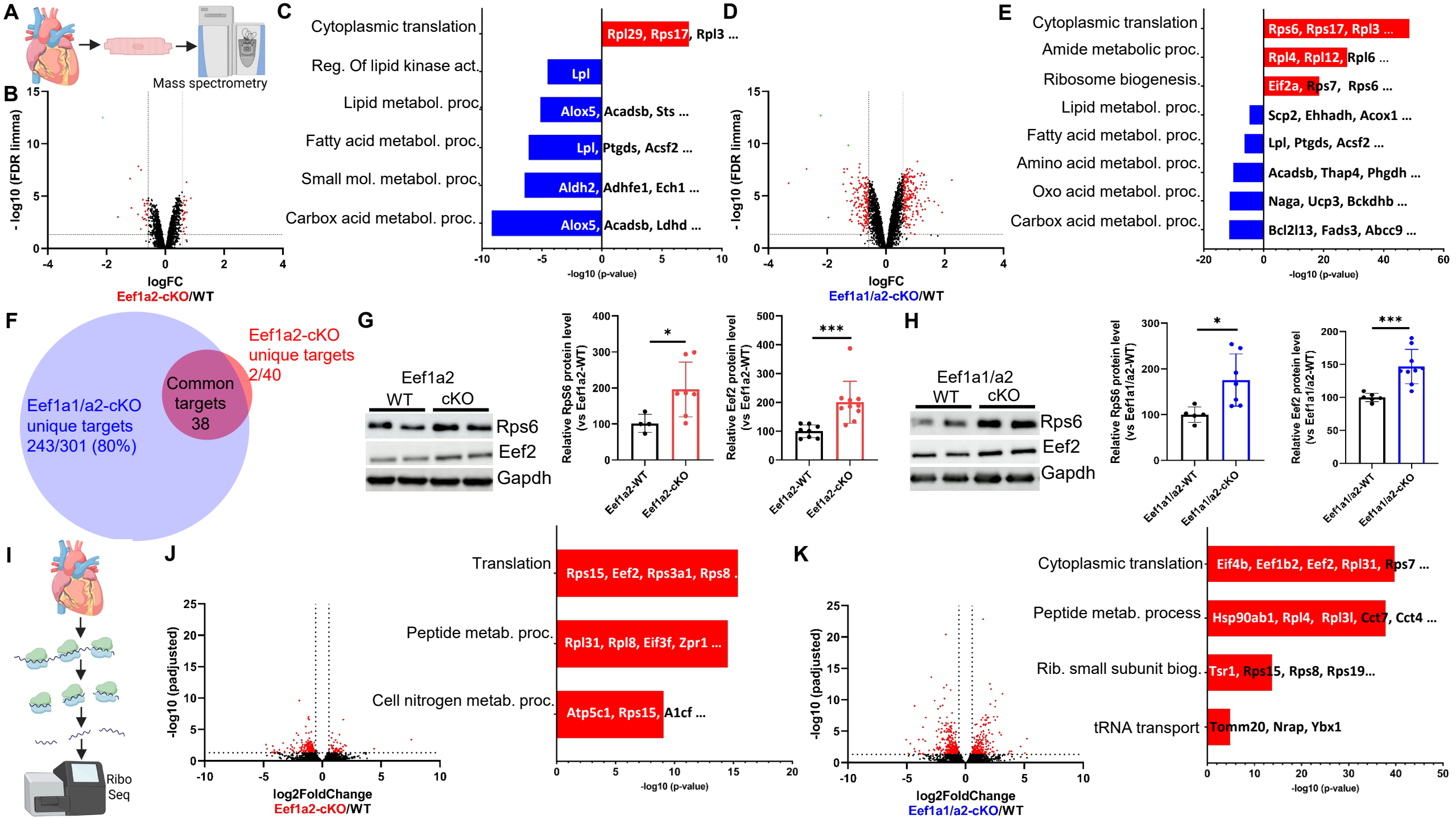
A
Mass spectrometry
B
- log10 (FDR limma)
logFC
Eef1a2-cKO/WT
C
Cytoplasmic translation
Reg. Of lipid kinase act.
Lipid metabol. proc.
Fatty acid metabol. proc.
Small mol. metabol. proc.
Carbox acid metabol. proc.
Rpl29, Rps17, Rpl3 ...
Lpl
Alox5, Acadsb, Sts ...
Lpl, Ptgds, Acsf2 ...
Aldh2, Adhfe1, Ech1 ...
Alox5, Acadsb, Ldhd ...
-log10 (p-value)
D
- log10 (FDR limma)
logFC
Eef1a1/a2-cKO/WT
E
Cytoplasmic translation
Amide metabolic proc.
Ribosome biogenesis.
Lipid metabol. proc.
Fatty acid metabol. proc.
Amino acid metabol. proc.
Oxo acid metabol. proc.
Carbox acid metabol. proc.
Rps6, Rps17, Rpl3 ...
Rpl4, Rpl12, Rpl6 ...
Eif2a, Rps7, Rps6 ...
Scp2, Ehhadh, Acox1 ...
Lpl, Ptgds, Acsf2 ...
Acadsb, Thap4, Phgdh ...
Naga, Ucp3, Bckdhb ...
Bcl2l13, Fads3, Abcc9 ...
-log10 (p-value)
F
Eef1a2-cKO
unique targets
2/40
Common
targets
38
Eef1a1/a2-cKO
unique targets
243/301 (80%)
G
Eef1a2
WT
cKO
Rps6
Eef2
Gapdh
Relative RpS6 protein level
(vs Eef1a2-WT)
Relative Eef2 protein level
(vs Eef1a2-WT)
Eef1a2-WT
Eef1a2-cKO
H
Eef1a1/a2
WT
cKO
Rps6
Eef2
Gapdh
Relative RpS6 protein level
(vs Eef1a1/a2-WT)
Relative Eef2 protein level
(vs Eef1a1/a2-WT)
Eef1a1/a2-WT
Eef1a1/a2-cKO
I
Ribo
Seq
J
-log10 (padjusted)
log2FoldChange
Eef1a2-cKO/WT
Translation
Peptide metab. proc.
Cell nitrogen metab. proc.
Rps15, Eef2, Rps3a1, Rps8 .
Rpl31, Rpl8, Eif3f, Zpr1 ...
Atp5c1, Rps15, A1cf ...
-log10 (p-value)
K
-log10 (padjusted)
log2FoldChange
Eef1a1/a2-cKO/WT
Cytoplasmic translation
Peptide metab. process
Rib. small subunit biog.
tRNA transport
Eif4b, Eef1b2, Eef2, Rpl31, Rps7 ...
Hsp90ab1, Rpl4, Rpl3l, Cct7, Cct4 ...
Tsr1, Rps15, Rps8, Rps19...
Tomm20, Nrap, Ybx1
-log10 (p-value)

Figure 3. Effects of cardiomyocyte-specific Eef1a2 and Eef1a1/a2 deletion on proteome and translation . (A) Schematic representation of the proteomic analysis workflow. (**B**) Volcano plot showing fold-change (FC; $\log_2$) and P value ($-\log_{10}$) of protein abundance changes in isolated cardiomyocytes from WT (n = 4) and Eef1a2-cKO (n = 4) mice at 1 month after Eef1a2 deletion. Candidate or hit proteins are highlighted in red.(**C**) Gene Ontology (GO) analysis of candidate and hit proteins identified in (B), shown as $-\log_{10}$(P value). Upregulated GO terms are shown in red and downregulated GO terms in blue. Example genes for each category are displayed in the panel. (**D**) Volcano plot showing fold-change (FC; $\log_2$) and P value ($-\log_{10}$) of protein abundance changes in isolated cardiomyocytes from WT (n = 4) and Eef1a1/a2-cKO (n = 4) mice at 1 month after Eef1a1/a2 deletion. Candidate or hit proteins are highlighted in red. (**E**) GO analysis of candidate and hit proteins identified in (D), shown as $-\log_{10}$(P value). (**F**) Venn diagram showing overlap of candidate and hit proteins identified in (B) and (D). (**G**) Representative Western blot analysis and quantification of RpS6 and Eef2 in isolated cardiomyocytes from Eef1a2-WT (RpS6, n = 4; Eef2, n = 8) and Eef1a2-cKO (RpS6, n = 7; Eef2, n = 10) mice. *P < 0.05, ***P < 0.001; unpaired t-test. (**H**) Representative Western blot analysis and quantification of RpS6 and Eef2 in isolated cardiomyocytes from Eef1a1/a2-WT (RpS6, n = 5; Eef2, n = 6) and Eef1a1/a2-cKO (RpS6, n = 7; Eef2, n = 9) mice. *P < 0.05, ***P < 0.001; unpaired t-test. (**I**) Schematic representation of the Ribo-seq analysis workflow. (**J**) Volcano plot showing fold-change (FC; $\log_2$) and P value ($-\log_{10}$) of changes in translation efficiency in cardiac tissue from WT (n = 4) and Eef1a2-cKO (n = 4) mice at 1 month after Eef1a2 deletion. Regulated genes are highlighted in red, with corresponding GO analysis shown as $-\log_{10}$(P value). (**K**) Volcano plot showing fold-change (FC; $\log_2$) and P value ($-\log_{10}$) of changes in translation efficiency in cardiac tissue from WT (n = 4) and Eef1a1/a2-cKO (n = 4) mice at 1 month after Eef1a1/a2 deletion. Regulated genes are highlighted in red, with corresponding GO analysis shown as $-\log_{10}$(P value).

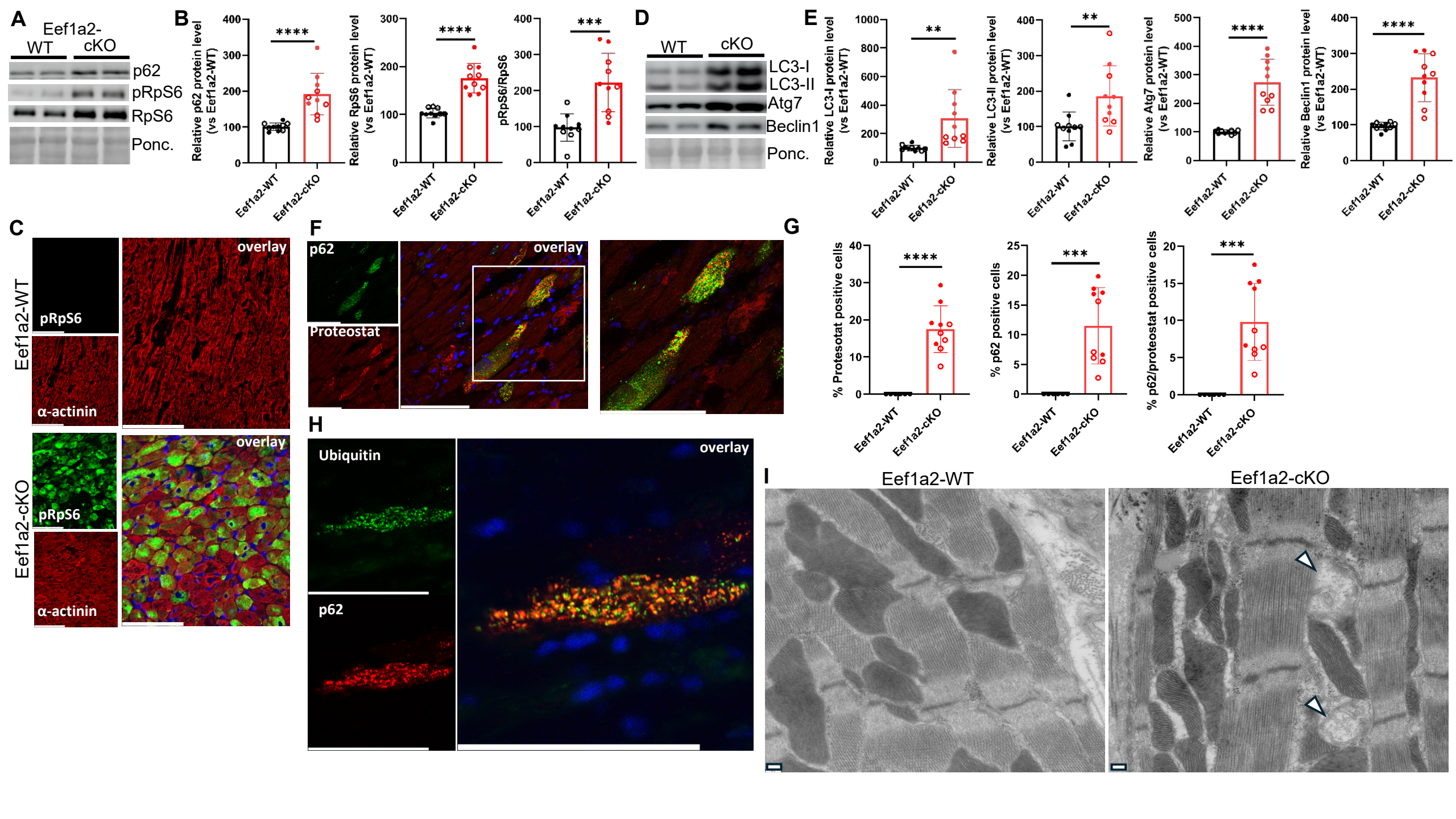
A
Eef1a2-
WT
cKO
p62
pRpS6
RpS6
Ponc.
B
Relative p62 protein level (vs Eef1a2-WT)
Relative RpS6 protein level (vs Eef1a2-WT)
pRpS6/RpS6
****
****
***
Eef1a2-WT
Eef1a2-cKO
D
WT
cKO
LC3-I
LC3-II
Atg7
Beclin1
Ponc.
E
Relative LC3-I protein level (vs Eef1a2-WT)
Relative LC3-II protein level (vs Eef1a2-WT)
Relative Atg7 protein level (vs Eef1a2-WT)
Relative Beclin1 protein level (vs Eef1a2-WT)
**
**
****
****
Eef1a2-WT
Eef1a2-cKO
C
Eef1a2-WT
Eef1a2-cKO
pRpS6
α-actinin
overlay
pRpS6
α-actinin
overlay
F
p62
Proteostat
overlay
G
% Protesotat positive cells
% p62 positive cells
% p62/proteostat positive cells
****
***
***
Eef1a2-WT
Eef1a2-cKO
H
Ubiquitin
p62
overlay
I
Eef1a2-WT
Eef1a2-cKO

Figure 4. Effects of cardiomyocyte-specific Eef1a2 deletion on autophaghy. (**A**) Representative Western blot analysis of p62, phosphorylated RpS6 (p-RpS6), and total RpS6 in cardiac tissue from Eef1a2-WT and Eef1a2-cKO mice at 2 months after Eef1a2 deletion. Ponceau (Ponc.) staining shows equal protein loading and blotting. (**B**) Quantification of the proteins shown in (A) from Eef1a2-WT (n = 9) and Eef1a2-cKO (n = 10) mice. ***P < 0.001, ****P < 0.0001; unpaired t-test. (**C**) Representative co-immunostaining of α-actinin (red) and p-RpS6 (green) in cardiac tissue from Eef1a2-WT or Eef1a2-cKO mice at 2 months after deletion (scale bars, 100 μm). (**D**) Representative Western blot analysis of LC3-I, LC3-II, Atg7, and Beclin1 in cardiac tissue from Eef1a2-WT and Eef1a2-cKO mice at 2 months after Eef1a2 deletion. (**E**) Quantification of the proteins shown in (D) from Eef1a2-WT (n = 9) and Eef1a2-cKO (n = 10) mice. **P < 0.01, ****P < 0.0001; unpaired t-test. (**F**) Representative co-immunostaining of Proteostat (red) and p62 (green) in cardiac tissue from Eef1a2-WT or Eef1a2-cKO mice at 2 months after deletion (left; scale bars, 100 μm). The right panel shows a magnified view of the boxed region (scale bar, 50 μm). (**G**) Quantification of Proteostat-positive (left), p62-positive (middle), and p62/Proteostat double-positive (right) cardiomyocytes from Eef1a2-WT (n = 6) and Eef1a2-cKO (n = 10) mice. ***P < 0.001, ****P < 0.0001; unpaired t-test. (**H**) Representative co-immunostaining of p62 (red) and ubiquitin (green) in cardiac tissue from Eef1a2-WT or Eef1a2-cKO mice at 2 months after deletion (scale bars, 50 μm). (**I**) Representative transmission electron microscopy images of cardiac tissue from Eef1a2-WT or Eef1a2-cKO mice at 2 months after deletion (scale bars, 200 nm).Filled circles denote males; open circles denote females.

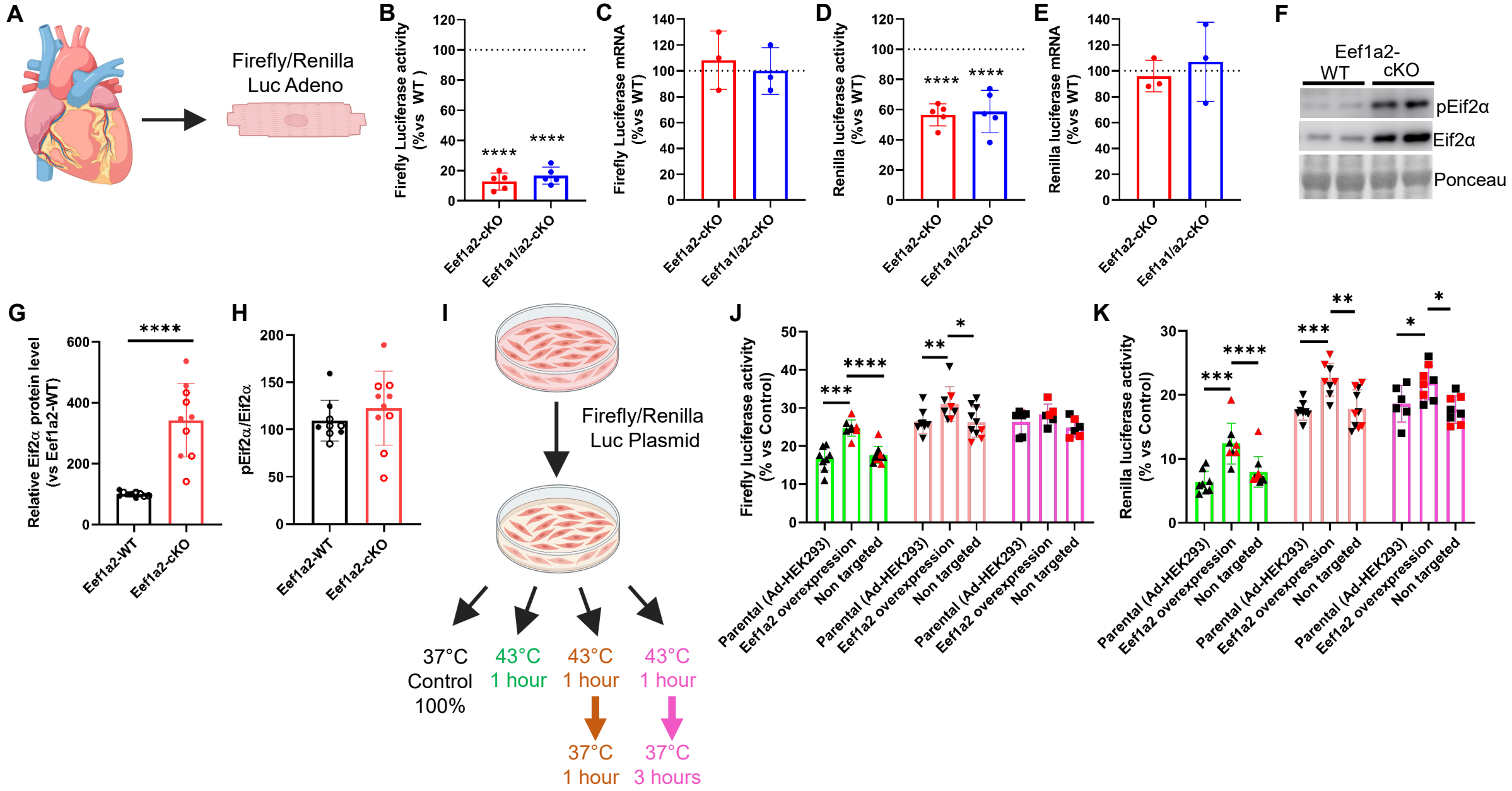
A
Firefly/Renilla
Luc Adeno
B
Firefly Luciferase activity
(%vs WT)
Eef1a2-cKO
Eef1a1/a2-cKO
C
Firefly Luciferase mRNA
(%vs WT)
D
Renilla luciferase activity
(%vs WT)
E
Renilla luciferase mRNA
(%vs WT)
F
Eef1a2-
WT
cKO
pEif2α
Eif2α
Ponceau
G
Relative Eif2α protein level
(vs Eef1a2-WT)
Eef1a2-WT
H
pEif2α/Eif2α
I
Firefly/Renilla
Luc Plasmid
37°C
Control
100%
43°C
1 hour
37°C
1 hour
37°C
3 hours
J
Firefly luciferase activity
(% vs Control)
Parental (Ad-HEK293)
Eef1a2 overexpression
Non targeted
K
Renilla luciferase activity
(% vs Control)

Figure 5. Effects of Eef1a2 on protein folding. (**A**) Schematic representation of the luciferase folding assay. Luc denotes luciferase. Adeno denotes Adenovirus. (**B**) Relative firefly luciferase activity measured in isolated cardiomyocytes from Eef1a2-cKO (n = 5) or Eef1a1/a2-cKO (n = 5) mice, normalized to their respective controls. (**C**) Relative mRNA expression of firefly luciferase in isolated cardiomyocytes from Eef1a2-cKO (n = 3) or Eef1a1/a2-cKO (n = 3) mice, normalized to their respective controls. (**D**) Relative Renilla luciferase activity measured in isolated cardiomyocytes from Eef1a2-cKO (n = 5) or Eef1a1/a2-cKO (n = 5) mice, normalized to their respective controls. (**E**) Relative mRNA expression of Renilla luciferase in isolated cardiomyocytes from Eef1a2-cKO (n = 3) or Eef1a1/a2-cKO (n = 3) mice, normalized to their respective controls. (**F**) Representative Western blot analysis of phosphorylated eIF2α (p-eIF2α) and total eIF2α in cardiac tissue from Eef1a2-WT and Eef1a2-cKO mice at 2 months after Eef1a2 deletion. (**G**) Quantification of total eIF2α expression in Eef1a2-WT (n = 10) and Eef1a2-cKO (n = 10) mice. ****P < 0.0001, unpaired t-test. (**H**) Quantification of the p-eIF2α/eIF2α ratio in Eef1a2-WT (n = 10) and Eef1a2-cKO (n = 10) mice. (**I**) Schematic representation of the protein unfolding/refolding assay. (**J**) Relative firefly luciferase activity measured in two independent Eef1a2-overexpressing clones (n = 4 each), two independent non-targeting control clones (n = 4 each), and parental cells (n = 8), normalized to their respective controls. *P < 0.05, **P < 0.01, ***P < 0.001, ****P < 0.0001; mixed-effects model followed by Tukey's multiple-comparison test. (**K**) Relative Renilla luciferase activity measured in the same clones and parental cells as in (J), normalized to their respective controls. *P < 0.05, **P < 0.01, ***P < 0.001, ****P < 0.0001; mixed-effects model followed by Tukey's multiple-comparison test. Filled circles denote males; open circles denote females.

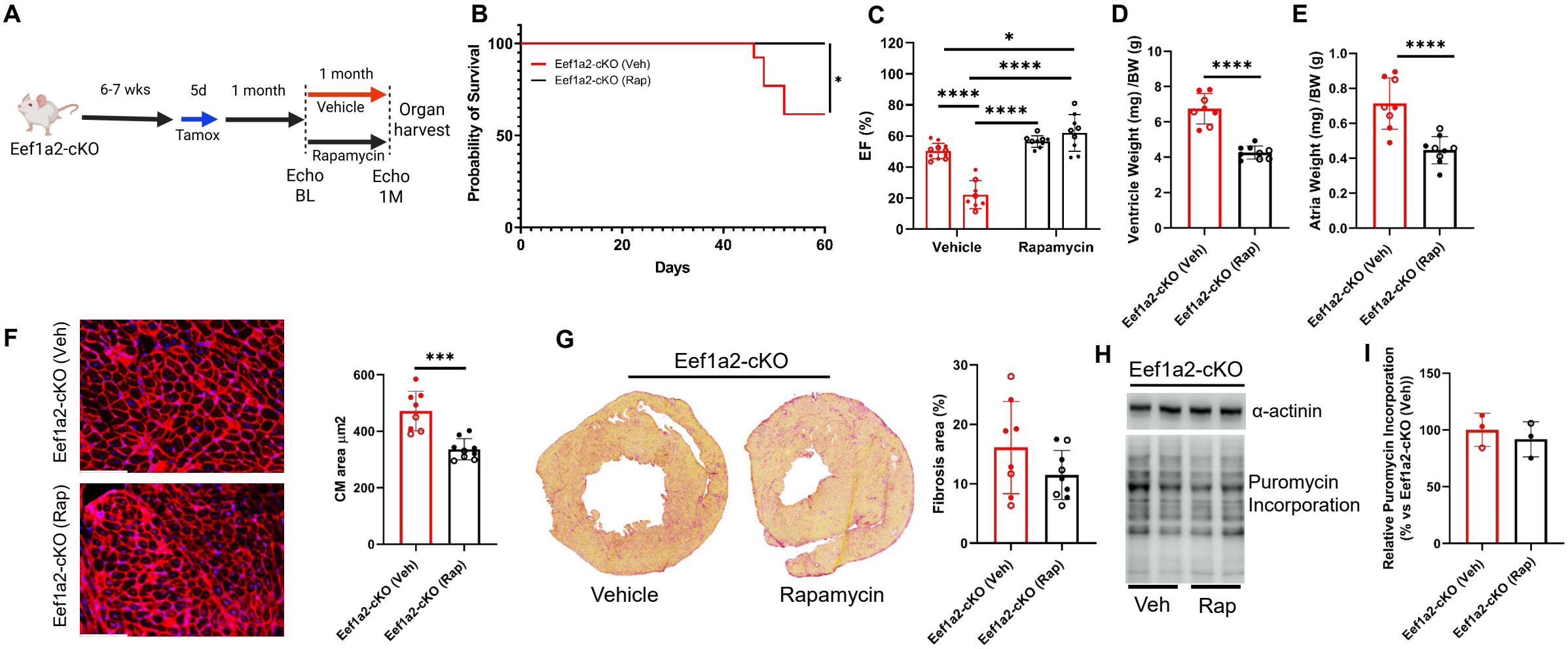
A
Eef1a2-cKO
6-7 wks
5d
Tamox
1 month
1 month
Vehicle
Rapamycin
Organ harvest
Echo BL
Echo 1M
B
Probability of Survival
Eef1a2-cKO (Veh)
Eef1a2-cKO (Rap)
Days
C
EF (%)
Vehicle
Rapamycin
D
Ventricle Weight (mg) /BW (g)
Eef1a2-cKO (Veh)
Eef1a2-cKO (Rap)
E
Atria Weight (mg) /BW (g)
Eef1a2-cKO (Veh)
Eef1a2-cKO (Rap)
F
Eef1a2-cKO (Veh)
Eef1a2-cKO (Rap)
CM area µm2
Eef1a2-cKO (Veh)
Eef1a2-cKO (Rap)
G
Eef1a2-cKO
Vehicle
Rapamycin
Fibrosis area (%)
Eef1a2-cKO (Veh)
Eef1a2-cKO (Rap)
H
Eef1a2-cKO
α-actinin
Puromycin Incorporation
Veh
Rap
I
Relative Puromycin Incorporation (% vs Eef1a2-cKO (Veh))
Eef1a2-cKO (Veh)
Eef1a2-cKO (Rap)

Figure 6. Effect of Rapamycin administration in Eef1a2-cKO mice. (A) Schematic representation of the rapamycin administration strategy. (**B**) Kaplan–Meier survival curves of vehicle-treated (n=13, 9/13 survived) or rapamycin-treated (n=9, 9/9 survived) Eef1a2-cKO mice. *P < 0.05, log-rank (Mantel–Cox) test. (**C**) Left ventricular ejection fraction in Eef1a2-cKO mice treated with vehicle (red bars) or rapamycin (black bars), measured before rapamycin administration (left bar, n = 11 and n = 9, respectively) and after 1 month of daily rapamycin treatment (right bar, n = 8 and n = 9, respectively). ****P < 0.0001, two-way ANOVA followed by Tukey's multiple-comparison test. (**D**) Ventricular weight relative to body weight in vehicle- (n = 8) or rapamycin-treated (n = 9) Eef1a2-cKO mice. ****P < 0.0001, unpaired t-test. (**E**) Atrial weight relative to body weight in vehicle- (n = 8) or rapamycin-treated (n = 9) Eef1a2-cKO mice. ****P < 0.0001, unpaired t-test. (**F**) Representative microscopic images of cardiac sections stained with wheat germ agglutinin (WGA) and corresponding quantification from vehicle- (n = 8) or rapamycin-treated (n = 9) Eef1a2-cKO mice. ***P < 0.001, unpaired t-test. (**G**) Representative Sirius Red staining of cardiac fibrosis and corresponding quantification from vehicle- (n = 8) or rapamycin-treated (n = 9) Eef1a2-cKO mice. (**H**) Representative Western blot analysis of puromycin incorporation in cardiac tissue from vehicle- or rapamycin-treated Eef1a2-cKO mice. (**I**) Quantification of puromycin incorporation in vehicle- (n = 3) or rapamycin-treated (n = 3) Eef1a2-cKO mice. Filled circles denote males; open circles denote females.

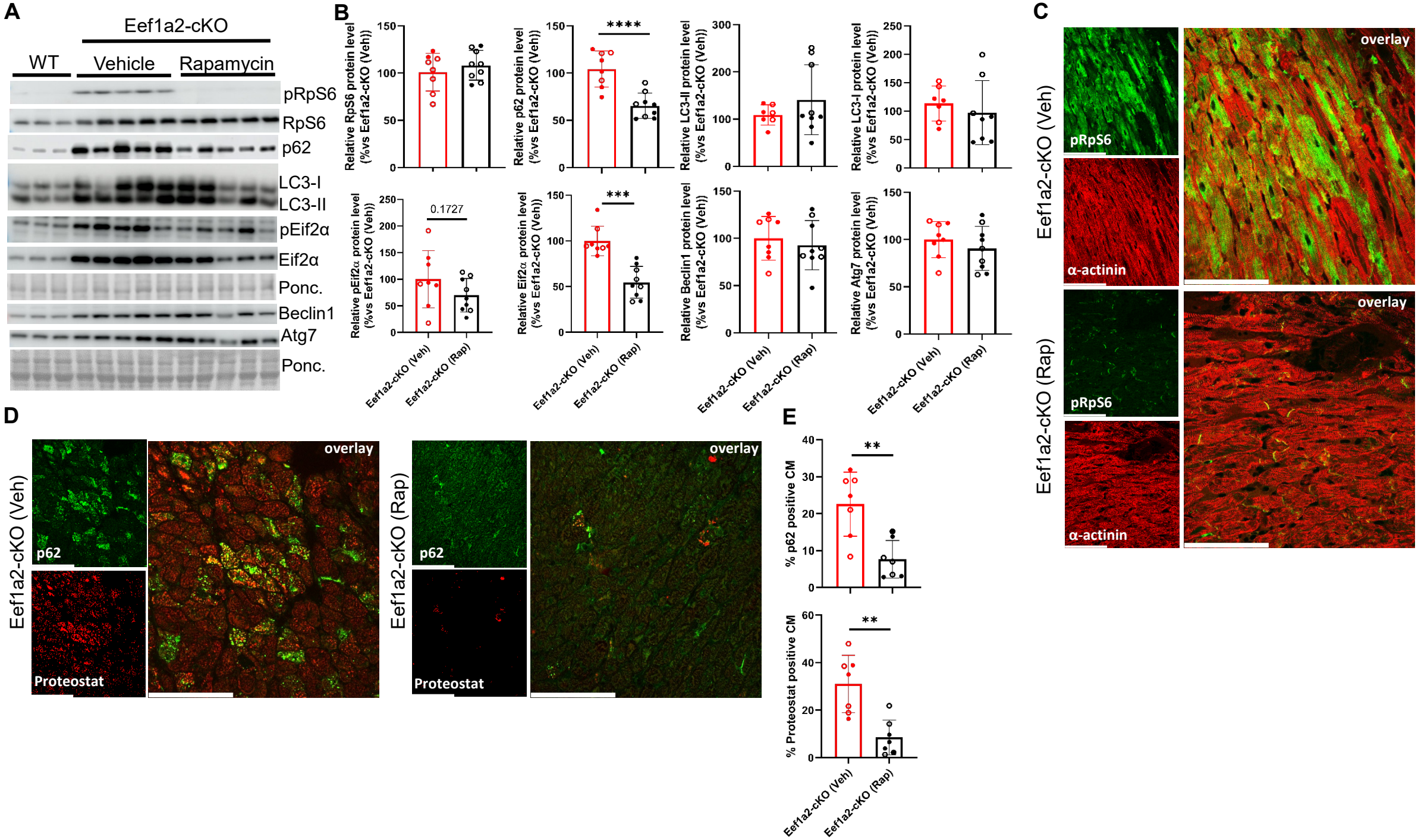
A
Eef1a2-cKO
WT
Vehicle
Rapamycin
pRpS6
RpS6
p62
LC3-I
LC3-II
pEif2α
Eif2α
Ponc.
Beclin1
Atg7
Ponc.
B
Relative RpS6 protein level (%vs Eef1a2-cKO (Veh))
Relative p62 protein level (%vs Eef1a2-cKO (Veh))
****
Relative LC3-II protein level (%vs Eef1a2-cKO (Veh))
Relative LC3-I protein level (%vs Eef1a2-cKO (Veh))
Relative pEif2α protein level (%vs Eef1a2-cKO (Veh))
0.1727
Relative Eif2α protein level (%vs Eef1a2-cKO (Veh))
***
Relative Beclin1 protein level (%vs Eef1a2-cKO (Veh))
Relative Atg7 protein level (%vs Eef1a2-cKO (Veh))
Eef1a2-cKO (Veh)
Eef1a2-cKO (Rap)
C
Eef1a2-cKO (Veh)
Eef1a2-cKO (Rap)
pRpS6
α-actinin
overlay
D
Eef1a2-cKO (Veh)
Eef1a2-cKO (Rap)
p62
Proteostat
overlay
E
% p62 positive CM
% Proteostat positive CM
**
Eef1a2-cKO (Veh)
Eef1a2-cKO (Rap)

Figure 7. Effect of rapamycin administration on altered proteostasis in Eef1a2-cKO mice. (**A**) Representative Western blot analysis of pRpS6, RpS6, p62, LC3-I, LC3-II, pEif2α, Eif2α, Beclin1, and Atg7 expression in cardiac tissue from vehicle- or rapamycin-treated Eef1a2-cKO mice. Ponceau (Ponc.) staining shows equal protein loading and blotting. (**B**) Quantification of protein expression shown in (A) in vehicle-treated (n = 8) or rapamycin-treated (n = 9) Eef1a2-cKO mice. ***P < 0.001, ****P < 0.0001; unpaired t-test. (**C**) Representative co-immunostaining of α-actinin (red) and pRpS6 (green) in cardiac tissue from vehicle- or rapamycin-treated Eef1a2-cKO mice (scale bars, 100 μm). (**D**) Representative co-immunostaining of Proteostat (red) and p62 (green) in cardiac tissue from vehicle- or rapamycin-treated Eef1a2-cKO mice (scale bars, 100 μm). (**E**) Quantification of p62-positive (upper panel) and Proteostat-positive (lower panel) cardiomyocytes in cardiac tissue from vehicle-treated (n = 7) or rapamycin-treated (n = 7) Eef1a2-cKO mice. **P < 0.01; unpaired t-test.Filled circles denote males; open circles denote females.

SUPPLEMENTAL MATERIAL

Gene	Forward	Reverse
Acta1	ATCCAGGCGGTGCTGTCCCT	ATGATGGCGTGTGGCAGGGC
Actc1	AGCCCTCTTTCATTGGTATGG	CCTCCAGATAGGACATTGTTGG
Nppa	TTCCTCGTCTTGGCCTTTTG	CCTCATCTTCTACCGGCATC
Nppb	GTCCAGCAGAGACCTCAAAA	AGGCAGAGTCAGAAACTGGA
Fhl1	GGCCAGTGAGACCTTTGTGT	GTGCCCTTGTACTCCACGTT
Fhl2	ACGAGACCTGCTTCACCTGT	TGCTCCCGGTAAGTAACACC
Myh6	GAGTGGGAGTTTATCGACTTCG	CCTTGACATTGCGAGGCTTC
Myh7	ACTGTCAACACTAAGAGGGTCA	TTGGATGATTTGATCTTCCAGGG
Firefly luciferase	AACGCTTCCATCTTCCAGGG	CCAGATCCACAACCTTCGCT
Renilla luciferase	GAACGTGCTGGACTCCTTCA	TTGCCGGACTTACCCATTCC
Eef1a1	CGTTCTTTTTCGCAACGGGT	TTCGATGGTTCGCTTGTCGA
Eef1a2	CAAGCGGACCATCGAGAAGT	GCCACGATCAGCACTGCG

Table S1: List of primers used for qRT-PCR (5´-3´).

Antibody	Vendor	Catalog number	Dilution
eEF1A1	Proteintech	11402-1-AP	WB: 1:2000
eEF1A2	Proteintech	16091-1-AP	WB: 1:2000
RpS6 (5G10)	Cell Signaling	# 2217	WB: 1:1000, IF: 1:100
pRpS6 (Ser235/236) (D57.2.2E)	Cell Signaling	# 4858	WB: 1:1000, IF: 1:100
eEF2	Cell Signaling	#2332	Cell Signaling
peEF2 (Thr56)	Cell Signaling	#2331	WB: 1:1000
p62/SQSTM1	Sigma	P0067	WB: 1:2000, IF: 1:200
LC3	Proteintech	14600-1-AP	WB: 1:1000
eIF2α	Cell Signaling	#9722	WB: 1:1000
peIF2α (Ser51) (D9G8)	Cell Signaling	#3398	WB: 1:1000
Atg7	Cell Signaling	#2631	WB: 1:1000
Beclin-1 (D40C5)	Cell Signaling	#3495	WB: 1:1000
EDF1	Proteintech	12419-1-AP	WB: 1:2000
α-Actinin (EA-53)	Sigma	A7811	IF: 1:200
Puromycin Antibody (12D10)	Sigma	MABE343	IF: 1:200
Wheat Germ Agglutinin (WGA)	Invitrogen	W21405	IF: 1:100
GAPDH (14C10)	Cell Signaling	#2118	WB: 1:1000
Ubiquitinylated proteins (FK2)	Sigma	04-263	IF: 1:100
Anti-mouse IgG, HRP-linked	Cell Signaling	#7076	WB: 1:1000
Anti-rabbit IgG, HRP-linked	Cell Signaling	#7074	WB: 1:1000
Anti-rabbit IgG (H+L), F(ab')2 Fragment (Alexa Fluor® 488 Conjugate)	Cell Signaling	#4412	IF: 1:200
Anti-rabbit IgG (H+L), F(ab')2 Fragment (Alexa Fluor® 555 Conjugate)	Cell Signaling	#4413	IF: 1:200
Anti-mouse IgG (H+L), F(ab')2 Fragment (Alexa Fluor® 488 Conjugate)	Cell Signaling	#4408	IF: 1:200
Anti-mouse IgG (H+L), F(ab')2 Fragment (Alexa Fluor® 555 Conjugate)	Cell Signaling	#4409	IF: 1:200

Table S2: List of antibodies used for Western blotting (WB) and immunofluorescence (IF) analyses.

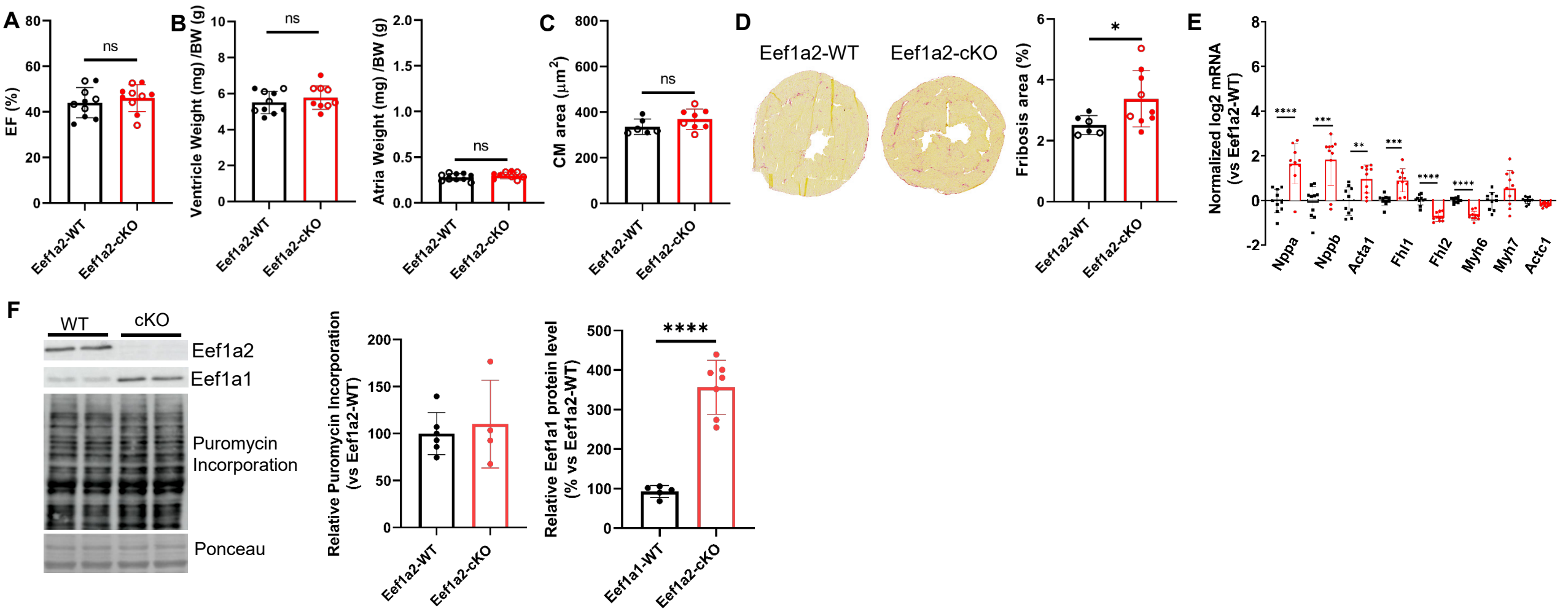

Figure S1. Effects of cardiomyocyte-specific Eef1a2 deletion at 1 month post tamoxifen.(**A**) Left ventricular ejection fraction of Eef1a2-WT (n = 10) and Eef1a2-cKO (n = 10) mice.(**B**) Ventricular (left) and atrial (right) weight normalized to body weight in Eef1a2-WT (n = 10) and Eef1a2-cKO (n = 9) mice at 1 month after Eef1a2 deletion. (**C**) Quantification of cardiomyocyte cross-sectional area after staining for wheat germ agglutinin (WGA) in Eef1a2-WT (n = 10) and Eef1a2-cKO (n = 10) mice at 1 month after Eef1a2 deletion.(**D**) Representative Sirius Red staining of cardiac fibrosis and corresponding quantification of fibrotic area from Eef1a2-WT (n = 6) and Eef1a2-cKO (n = 9) mice at 1 month after Eef1a2 deletion. *P < 0.05, unpaired t-test. (**E**) Normalized mRNA expression levels of selected genes in cardiac tissue from Eef1a2-WT (n = 10) and Eef1a2-cKO (n = 10) mice at 1 month after Eef1a2 deletion. **P < 0.01, ***P < 0.001, ****P < 0.0001; unpaired t-test.(**F**) Representative Western blots (left) of isolated cardiomyocytes at 2 months after Eef1a2 deletion. Ponceau staining shows equal protein loading and blotting. Right: Quantification of puromycin incorporation and Eef1a1 protein levels in isolated cardiomyocytes from Eef1a2-WT (n = 5) and Eef1a2-cKO (n = 4 for puromycin incorporation and n=7 for Eef1a1) mice from independent isolations at 1 month after Eef1a2 deletion.****P < 0.0001; unpaired t-test. Filled circles denote males; open circles denote females.

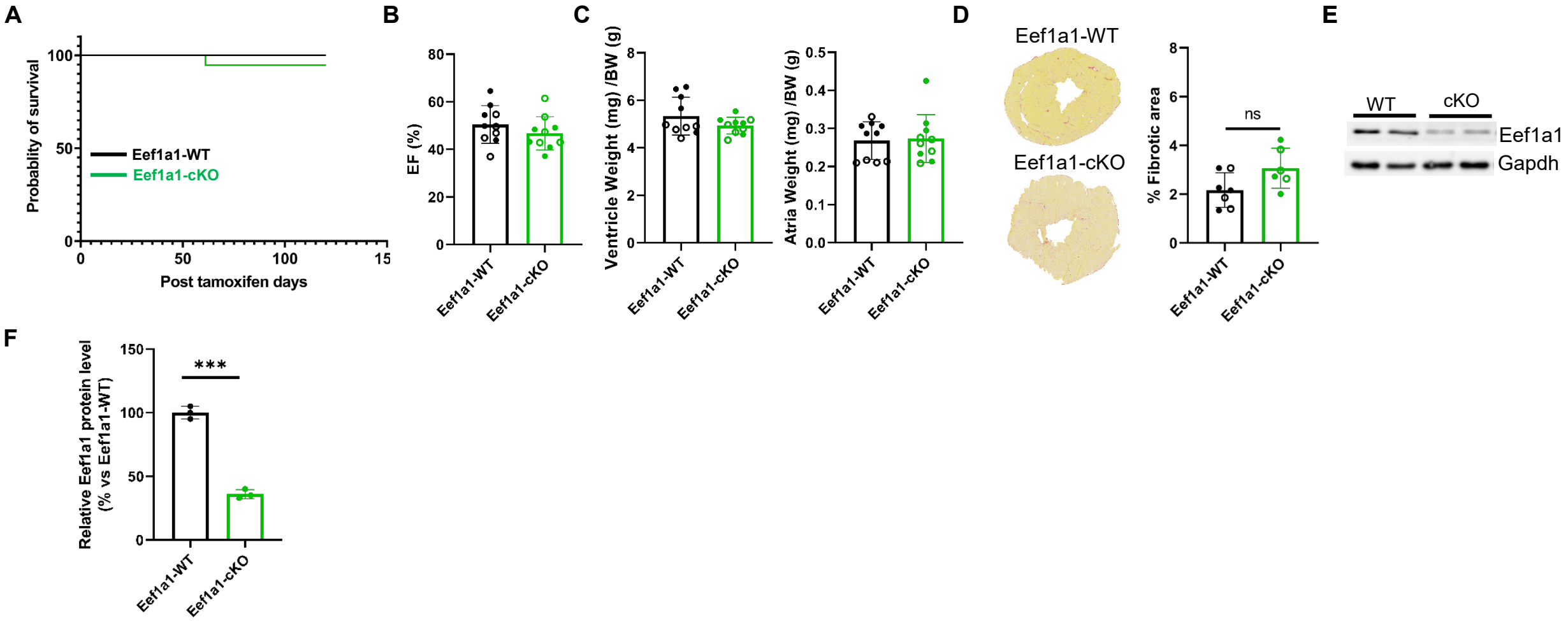

Figure S2. Effects of cardiomyocyte-specific Eef1a1 deletion. (**A**) Kaplan–Meier survival curves of Eef1a1-WT (n = 10, 10/10 survived) and Eef1a1-cKO (n = 15, 14/15 survived) mice. (**B**) Left ventricular ejection fraction of Eef1a1-WT and Eef1a1-cKO at 4 months after Eef1a1 deletion. (**C**) Ventricular (left) and atrial (right) weight normalized to body weight in Eef1a1-WT and Eef1a1-cKO mice at 4 months after Eef1a1deletion. (**D**) Representative Sirius Red staining of cardiac fibrosis and corresponding quantification of fibrotic area from Eef1a1-WT (n=7) and Eef1a1-cKO (n=6) mice at 4 months after Eef1a1 deletion. (**E**) Representative Western blot analysis of isolated cardiomyocytes at 1 months after Eef1a1 deletion.(**F**) Quantification of Eef1a1 protein level in isolated cardiomyocytes from Eef1a1-WT (n = 3) and Eef1a1-cKO (n = 3) mice from independent isolations at 1 month after Eef1a1 deletion. Filled circles denote males; open circles denote females.

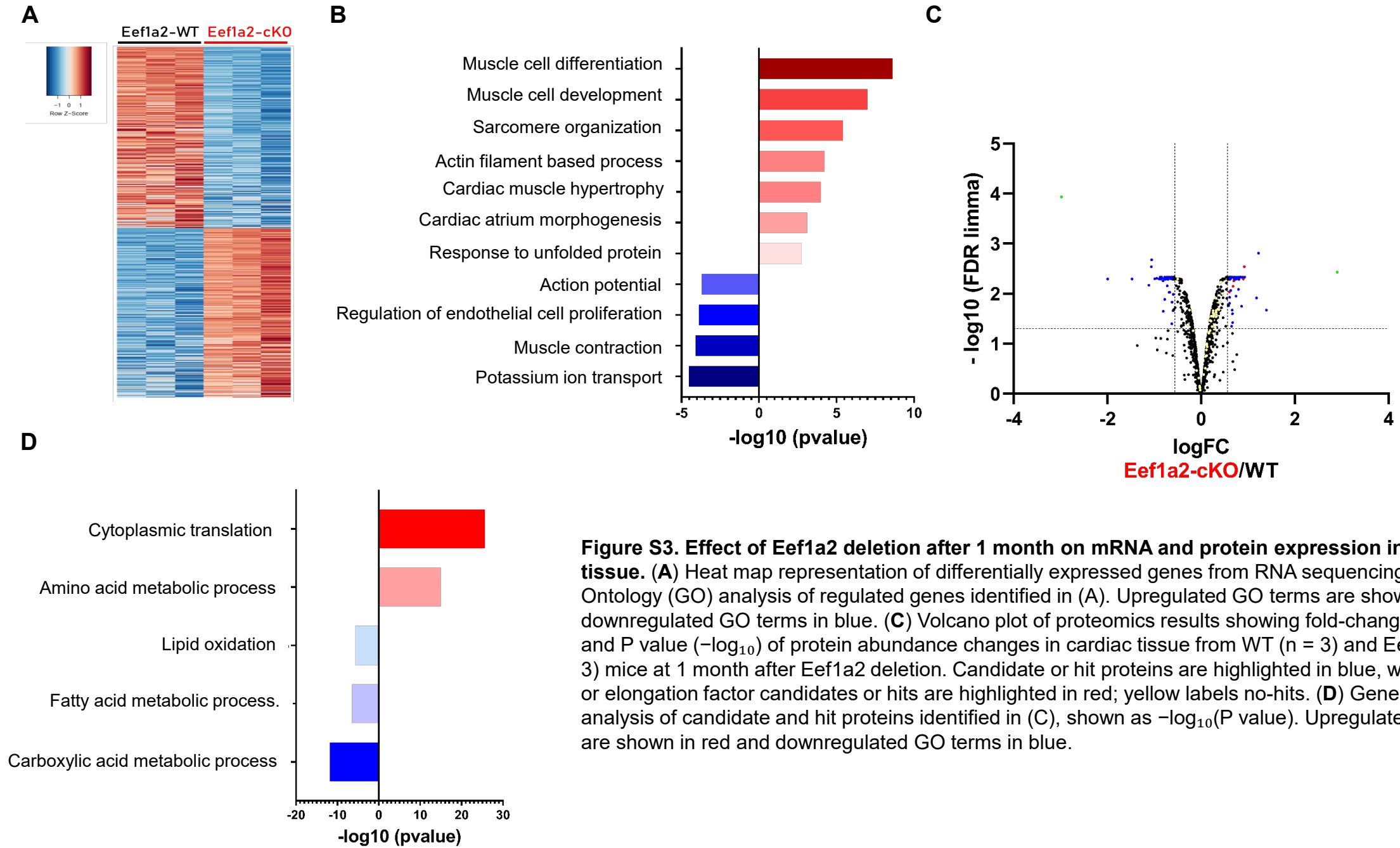

Figure S3. Effect of Eef1a2 deletion after 1 month on mRNA and protein expression in cardiac tissue. (**A**) Heat map representation of differentially expressed genes from RNA sequencing. (**B**) Gene Ontology (GO) analysis of regulated genes identified in (A). Upregulated GO terms are shown in red and downregulated GO terms in blue. (**C**) Volcano plot of proteomics results showing fold-change (FC; $\log_2$) and P value ($-\log_{10}$) of protein abundance changes in cardiac tissue from WT (n = 3) and Eef1a2-cKO (n = 3) mice at 1 month after Eef1a2 deletion. Candidate or hit proteins are highlighted in blue, while ribosomal or elongation factor candidates or hits are highlighted in red; yellow labels no-hits. (**D**) Gene Ontology (GO) analysis of candidate and hit proteins identified in (C), shown as $-\log_{10}$(P value). Upregulated GO terms are shown in red and downregulated GO terms in blue.

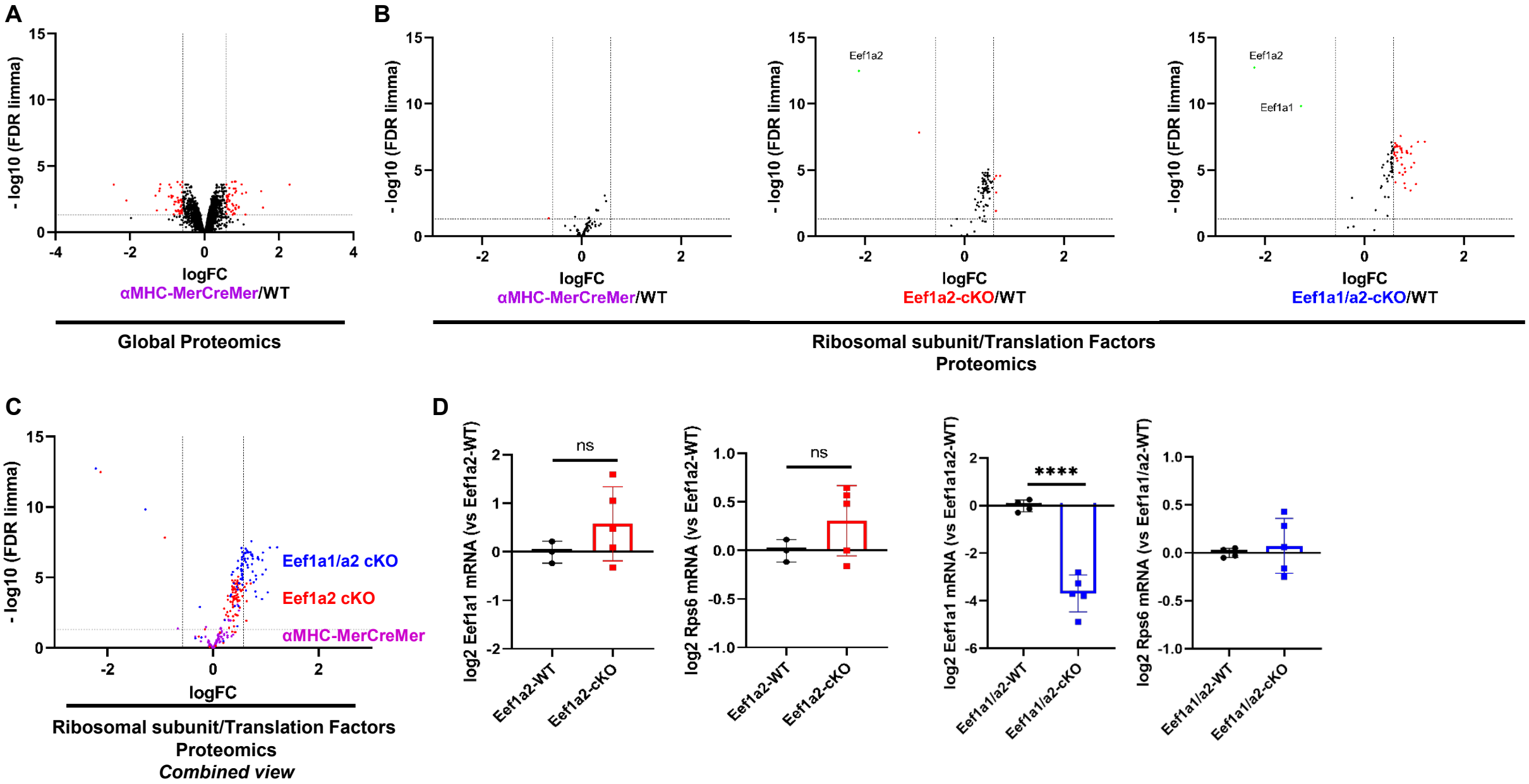
A
- log10 (FDR limma)
logFC
αMHC-MerCreMer/WT
Global Proteomics
B
αMHC-MerCreMer/WT
Eef1a2
Eef1a2-cKO/WT
Eef1a1
Eef1a1/a2-cKO/WT
Ribosomal subunit/Translation Factors Proteomics
C
Eef1a1/a2 cKO
Eef1a2 cKO
αMHC-MerCreMer
Ribosomal subunit/Translation Factors Proteomics
Combined view
D
log2 Eef1a1 mRNA (vs Eef1a2-WT)
log2 Rps6 mRNA (vs Eef1a2-WT)
log2 Eef1a1 mRNA (vs Eef1a1a2-WT)
log2 Rps6 mRNA (vs Eef1a1/a2-WT)
ns
****
Eef1a2-WT
Eef1a2-cKO
Eef1a1/a2-WT
Eef1a1/a2-cKO

Figure S4. Effect of Eef1a2 deletion after 1 month on ribosomal and translation factor protein and mRNA expression of isolated cardiomyocytes. (**A**) Volcano plot showing fold-change (FC; $\log_2$) and P value ($-\log_{10}$) of protein abundance changes in isolated cardiomyocytes from WT (n = 4) and MerCreMer (n = 4) mice at 1 month after tamoxifen injection. (**B**) Volcano plot showing fold-change (FC; $\log_2$) and P value ($-\log_{10}$) ribosomal and translation factor changes in in isolated cardiomyocytes from WT (n = 4), αMHC-MerCreMer (n=4), Eef1a2-cKO (n=4) and Eef1a1/a2-cKO (n = 4) mice at 1 month after tamoxifen injection. Candidate or hit proteins are highlighted in red. (**C**) Volcano plot representation of the combined data shown in (B). (**D**) mRNA expression levels of Eef1a1 and Rps6 in 4 independent cardiomyocyte isolations from Eef1a2-cKO mice (left panels) and Eef1a1/a2-cKO mice (right panels).

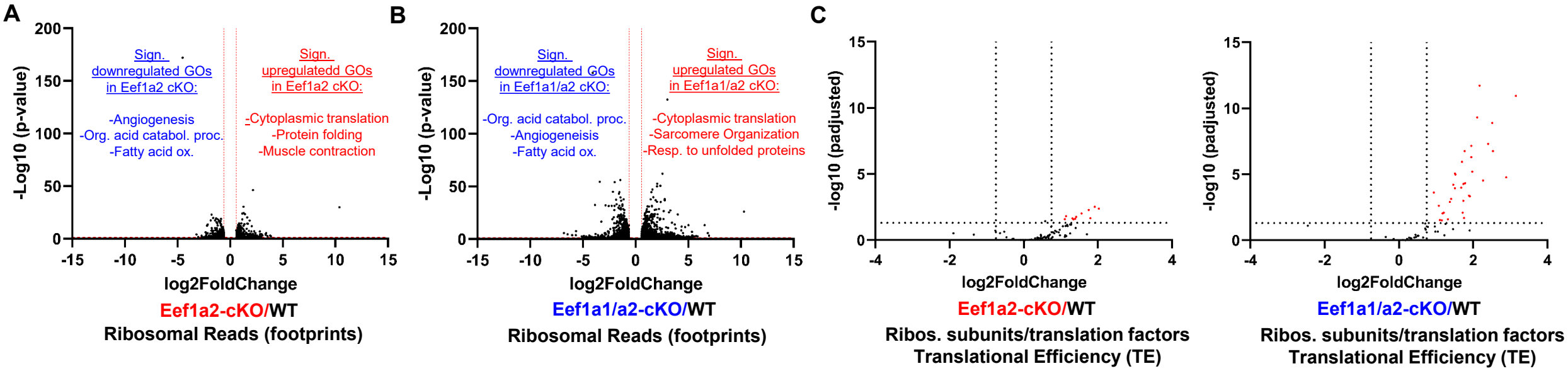

Figure S5. Effect of Eef1a on translation efficiency in cardiac tissue. (**A**) Volcano plot showing fold-change (FC; $\log_2$) and P value ($-\log_{10}$) of changes in ribosomal footprints in cardiac tissue from WT (n = 4) and Eef1a2-cKO (n = 4) mice at 1 month after Eef1a2 deletion. Significantly upregulated GO terms are shown in red, whereas downregulated terms are shown in blue. (**B**) Volcano plot showing fold-change (FC; $\log_2$) and P value ($-\log_{10}$) of changes in ribosomal footprints in cardiac tissue from WT (n = 4) and Eef1a1/a2-cKO (n = 4) mice at 1 month after Eef1a1/a2 deletion. Significantly upregulated GO terms are shown in red, whereas downregulated terms are shown in blue. (**C**) Volcano plot showing fold change (FC; $\log_2$) and P value ($-\log_{10}$) of changes in translation efficiency of ribosomal subunits and translation factors in cardiac tissue from WT (n = 4), Eef1a2-cKO (n = 4), and Eef1a1/a2-cKO (n = 4) mice at 1 month after tamoxifen injection. Regulated genes are highlighted in red.

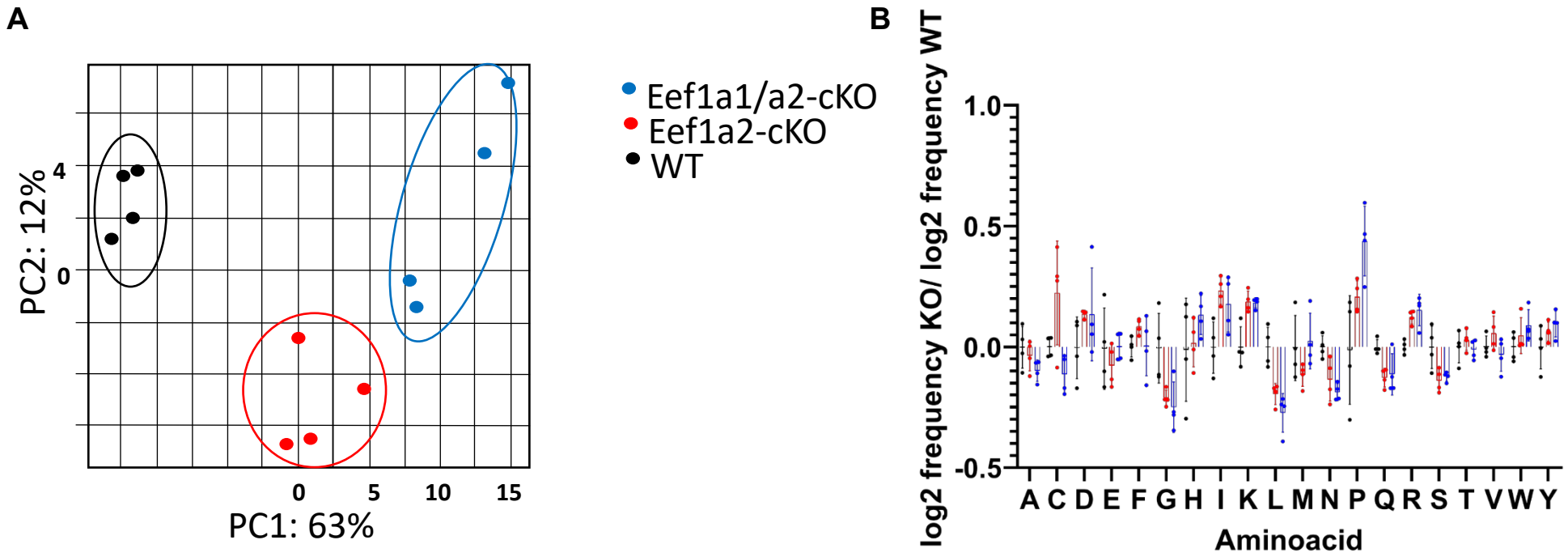

Figure S6. Codon occupancy in cardiac tissue 1 month after Eef1a2 or Eef1a1/a2 deletion.(**A**) Principal Component Analysis (PCA) showing clustering of the different experimental groups.(**B**) P-site amino acid occupancy of individual amino acids in cardiac tissue.

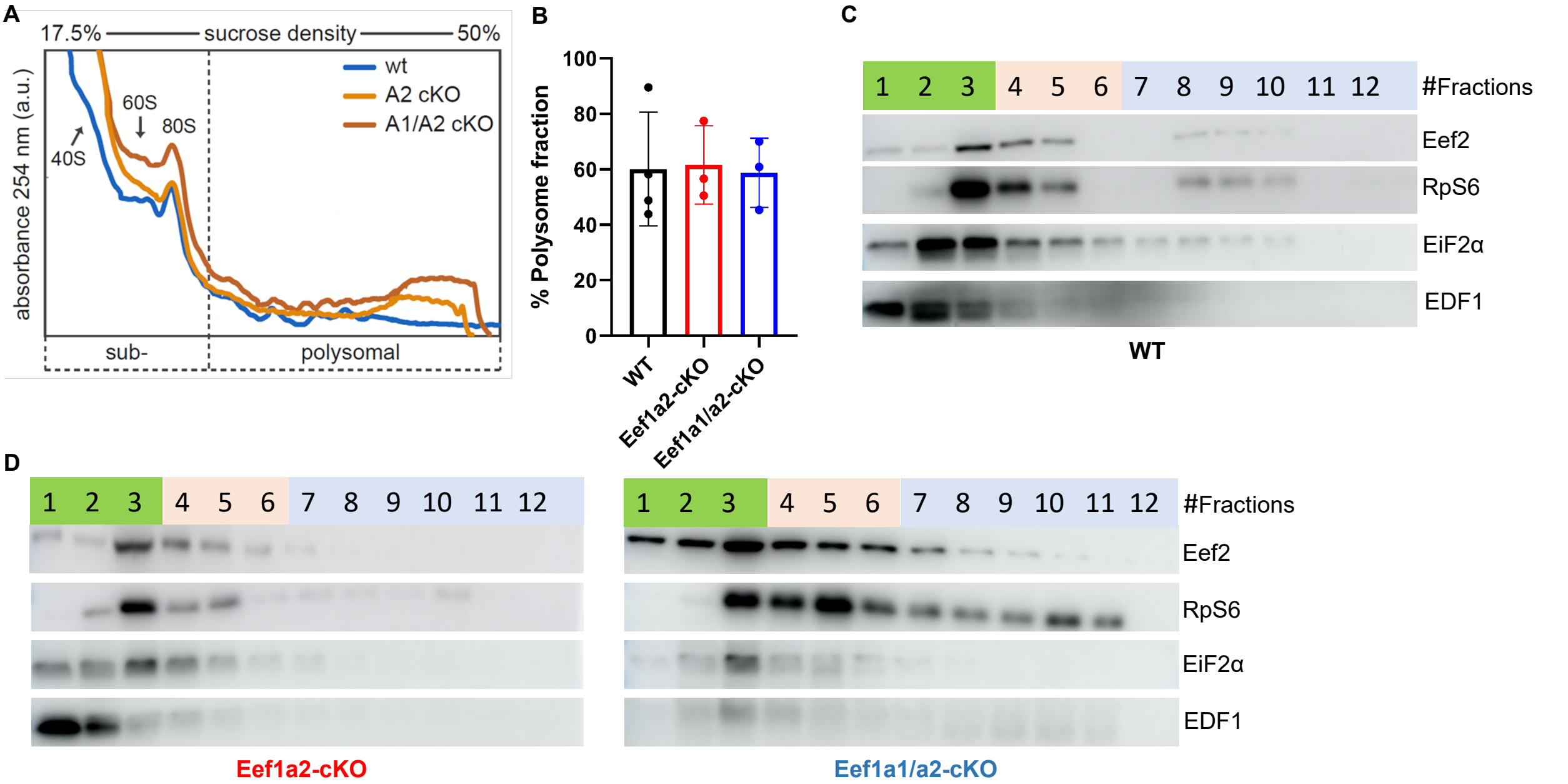

Figure S7. Polysome profiling of WT, Eef1a2-cKO, and Eef1a1/a2-cKO cardiac tissue 1 month after tamoxifen. (**A**) Representative monosome/polysome profiles.(**B**) Quantification of polysome fractions from WT (n = 3), Eef1a2-cKO (n = 3), and Eef1a1/a2-cKO (n = 3) cardiac tissue.(**C**) Representative Western blot of Eef2, RpS6, Eif2α, and EDF1 in fractions collected from WT cardiac tissue. (**D**) Same analysis as in (C) for Eef1a2-cKO (left) and Eef1a1/a2-cKO (right) cardiac tissue.

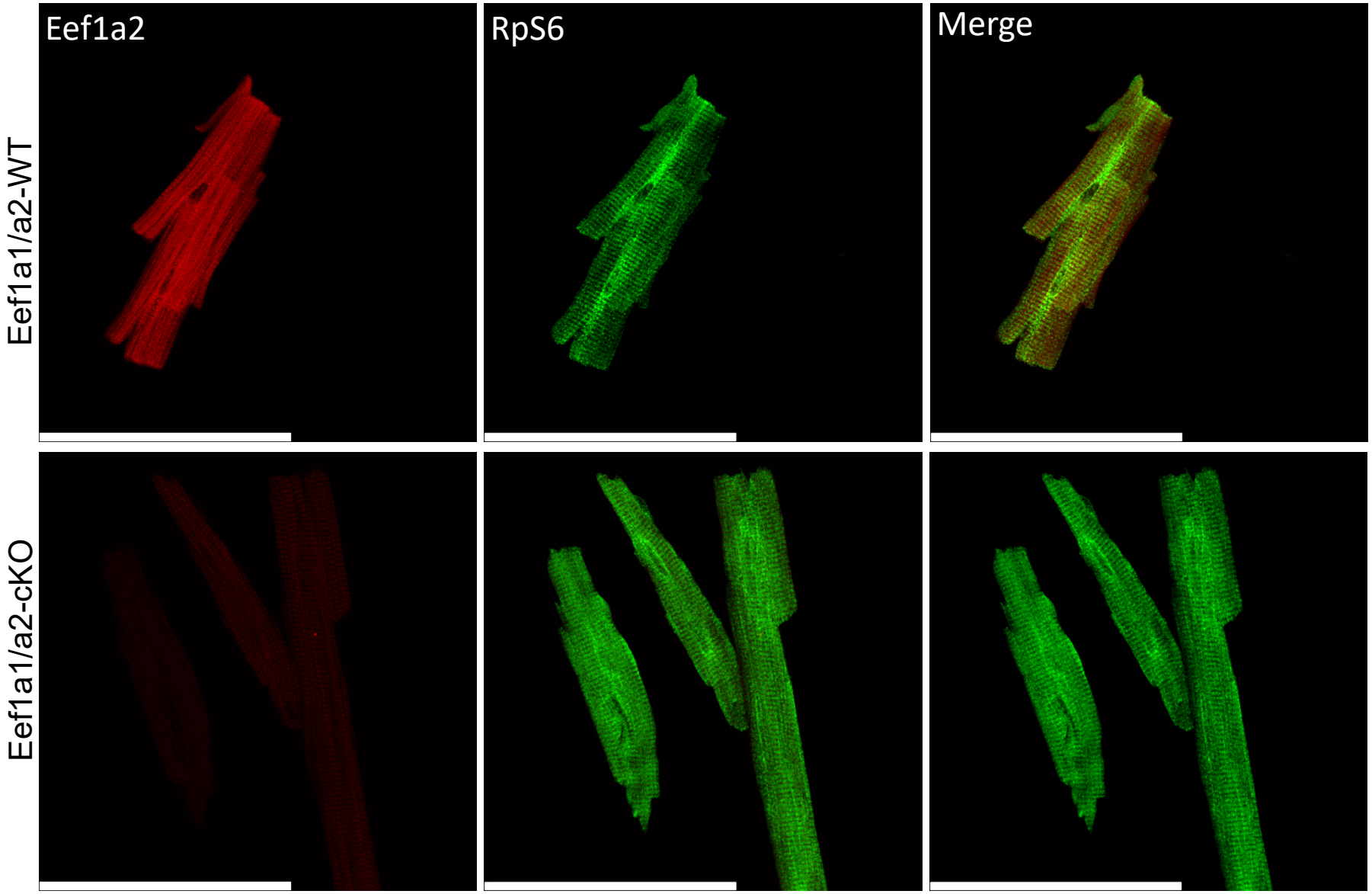

Figure S8. Representative co-immunostaining of Eef1a (red) and RpS6 (green) in isolated cardiomyocytes from Eef1a1/a2-WT or Eef1a1/a2-cKO mice at 1 month after tamoxifen. Upper panel: WT isolated cardiomyocytes. Lower panel: Eef1a1/a2-cKO isolated cardiomyocytes. Scale bars: 100μm.

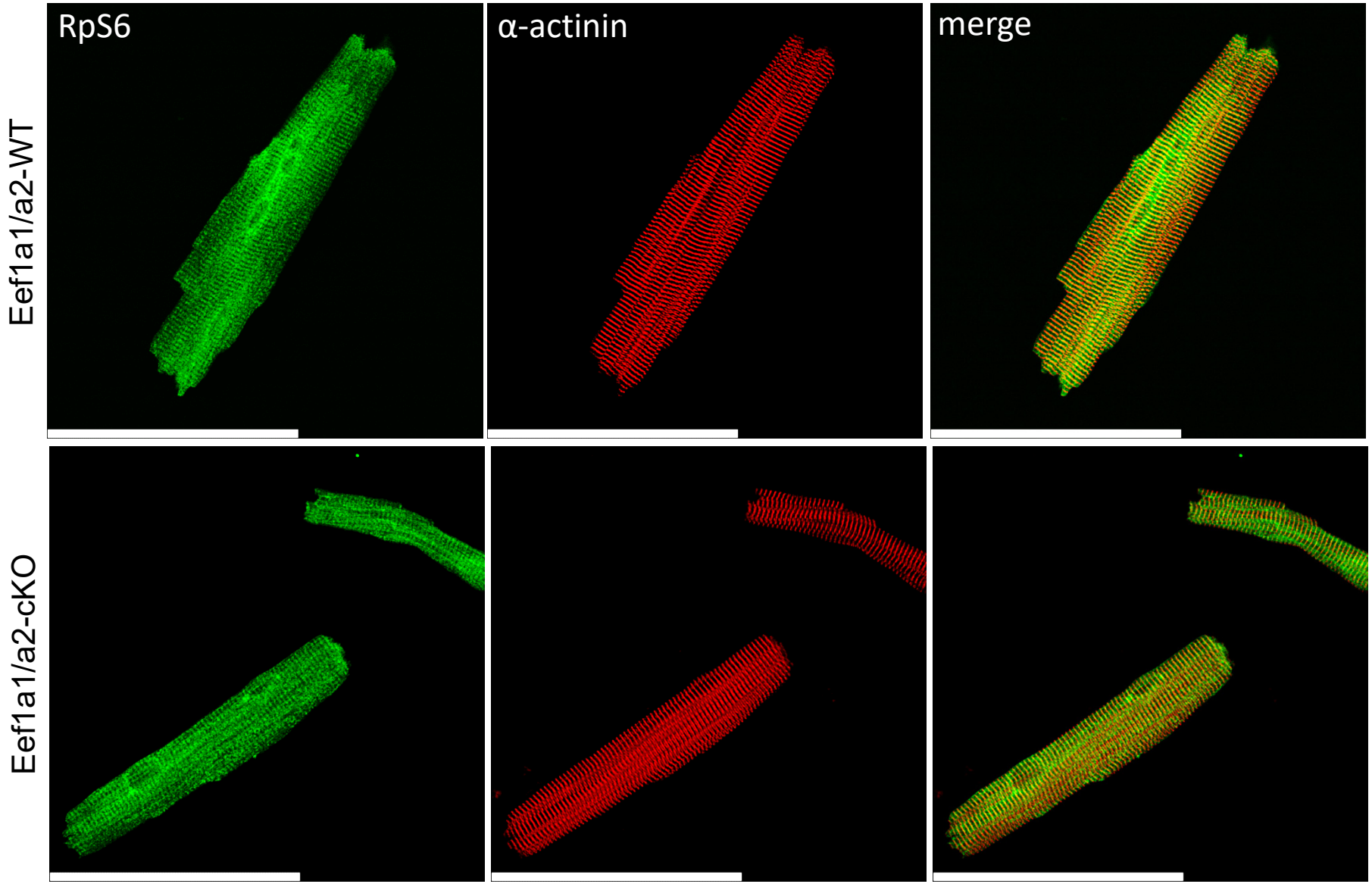

Figure S9 . Representative co-immunostaining of α-actinin (red) and RpS6 (green) in isolated cardiomyocytes from Eef1a1/a2-WT or Eef1a1/a2-cKO mice at 1 month after deletion. Upper panel: WT isolated cardiomyocytes. Lower panel: Eef1a1/a2-cKO isolated cardiomyocytes. Scale bars: 100μm.

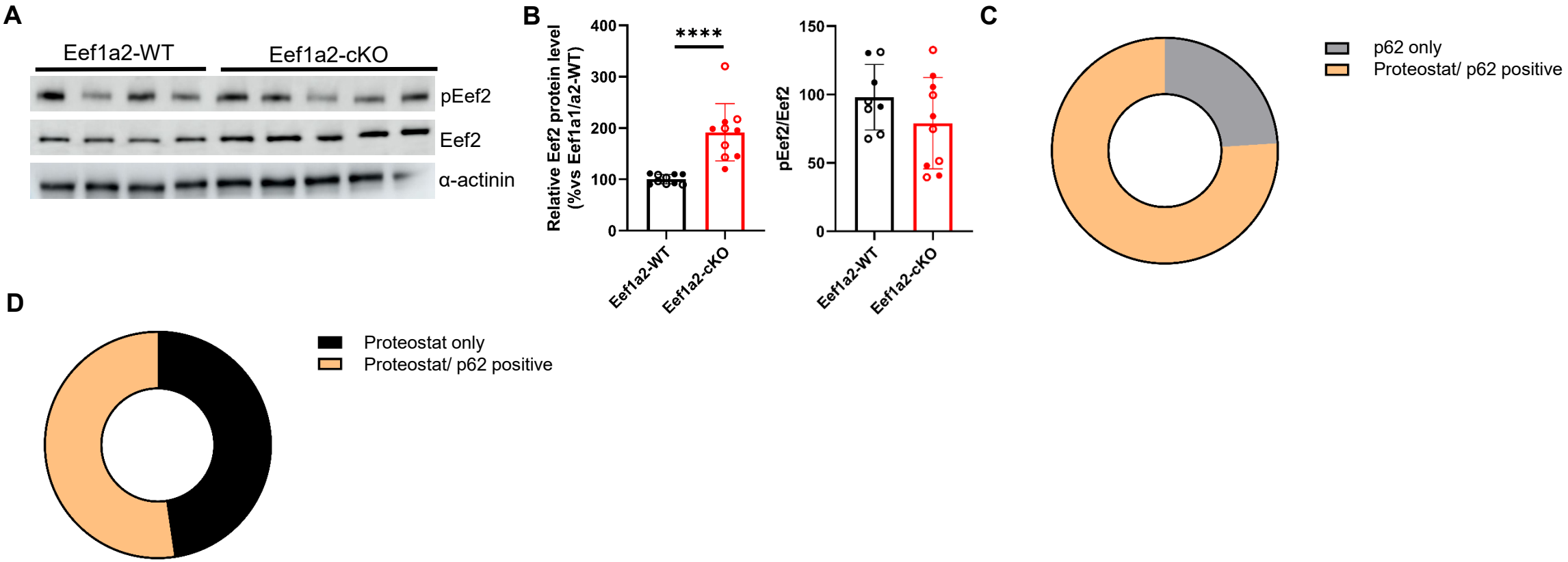

Figure S10. Western blot and autophagy analysis in Eef1a2-cKO cardiac tissue. (**A**) Representative Western blot analysis of pEef2, Eef2, and α-actinin in cardiac tissue from Eef1a2-WT and Eef1a2-cKO mice at 2 months after Eef1a2 deletion. (**B**) Quantification of protein levels shown in (A) from Eef1a2-WT (n = 9) and Eef1a2-cKO (n = 10) mice. ****P < 0.0001; unpaired t-test. (**C**) Circle representation of p62-positive cardiomyocytes alone or co-stained with Proteostat in Eef1a2-cKO hearts. (**D**) Circle representation of Proteostat-positive cardiomyocytes alone or co-stained with p62 in Eef1a2-cKO hearts. Filled circles denote males; open circles denote females.

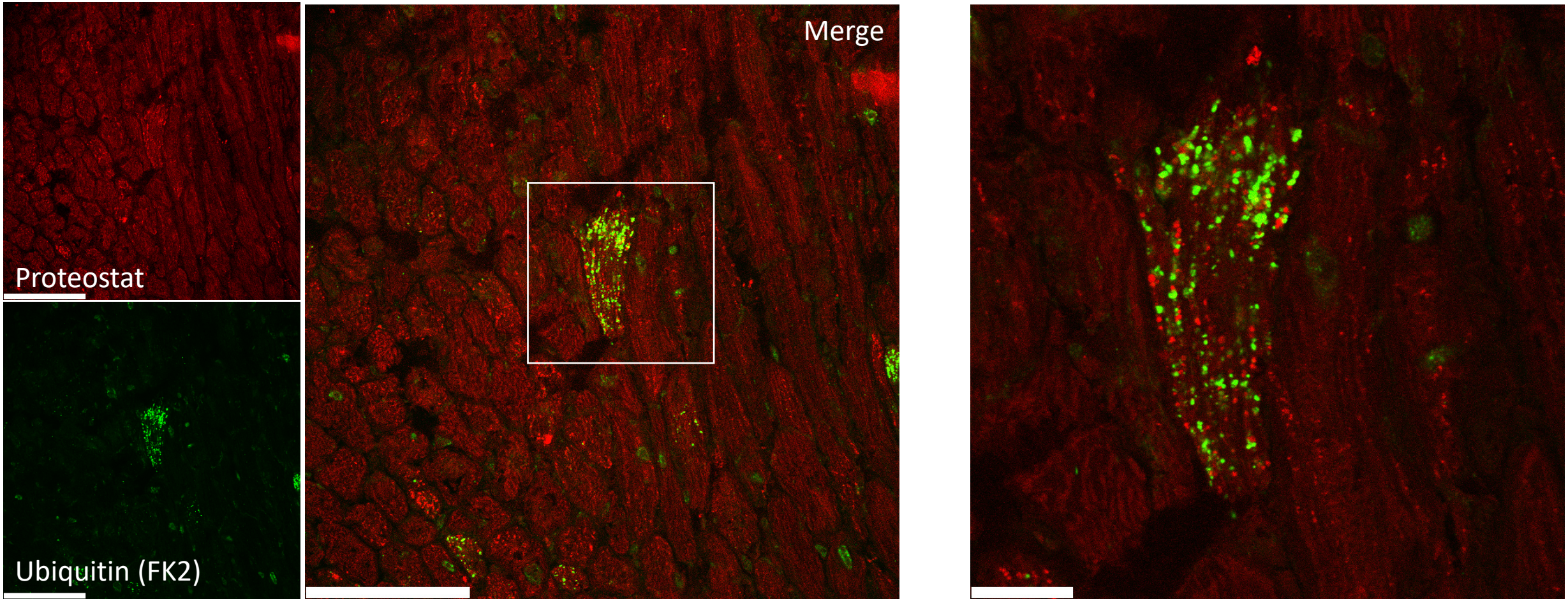

Figure S11. Representative co-staining of Proteostat (red) and Ubiquitin (green) in hearts of Eef1a2-cKO mice. The right panel shows a magnified version of the boxed region. Scale bars: 100μm in the left three panels, 20μm in the right panel.

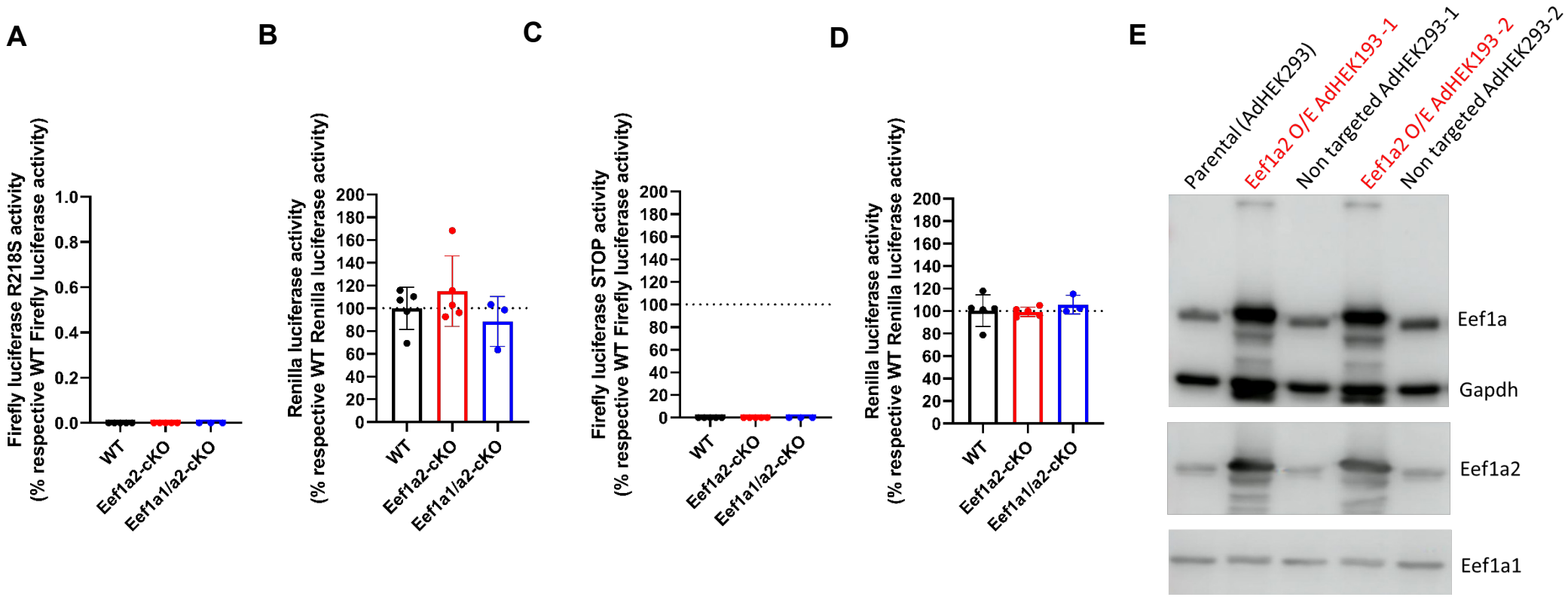

Figure S12. Effect of Eef1a2 on protein translation fidelity. (A) Relative firefly R218S luciferase activity measured in isolated cardiomyocytes from Eef1a2-cKO (n = 5) or Eef1a1/a2-cKO (n = 5) mice, normalized to their respective wild-type controls.(**B**) Relative Renilla luciferase activity corresponding to the samples in (A).(**C**) Relative firefly STOP luciferase activity measured in isolated cardiomyocytes from Eef1a2-cKO (n = 5) or Eef1a1/a2-cKO (n = 5) mice, normalized to their respective wild-type controls.(**D**) Relative Renilla luciferase activity corresponding to the samples in (C).(**E**) Representative Western blot of Eef1a2-overexpressing and non-targeted clones used in the folding/unfolding assay.

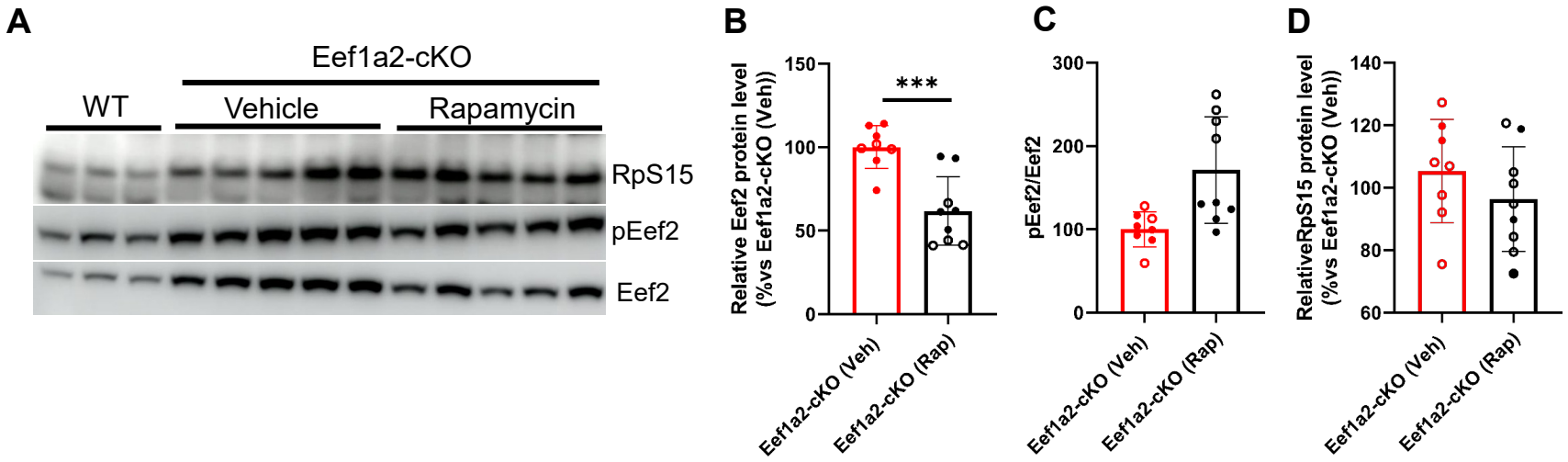

Figure S13. Western blot analysis in cardiac tissue from vehicle- or Rapamycin-treated Eef1a2-cKO mice. (A) Representative Western blot analysis of RpS15, Eef2, and pEef2 in cardiac tissue from vehicle- or rapamycin-treated Eef1a2-cKO mice. (**B, C and D**) Quantification of protein expression shown in (A) in vehicle-treated (n = 8) or rapamycin-treated (n = 9) Eef1a2-cKO mice. ***P < 0.001, unpaired t-test.